ผลของความบกพร่องภายในและพื้นผิวของตัวรองรับไทเทเนียที่มีต่อคุณลักษณะและสมบัติการเป็น
ตัวเร่งปฏิกิริยาของตัวเร่งปฏิกิริยาโคบอลต์บนตัวรองรับไทเทเนียด้วยปฏิกิริยาเมทาเนชัน

นางสาวสุภาวรรณ ศุภวาณิชย์มงคล

EFFECTS OF BULK AND SURFACE DEFECTS OF TiO$_2$ SUPPORT ON THE
PHYSICO-CHEMICAL PROPERTIES OF Co/TiO$_2$ CATALYST VIA
METHANATION

Miss Supawan Supawanitchmongkol

A Thesis Submitted in Partial Fulfillment of the Requirements
for the Degree of Master of Engineering Program in Chemical Engineering
Department of Chemical Engineering
Faculty of Engineering
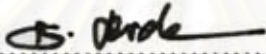Chulalongkorn University
Academic Year 2007

Thesis Title   EFFECTS OF BULK AND SURFACE DEFECTS OF TiO₂ SUPPORT ON THE PHYSICO-CHEMICAL PROPERTIES OF Co/TiO₂ CATALYST VIA METHANATION
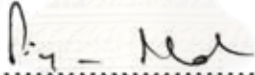
By   Miss Supawan Supawanitchmongkol
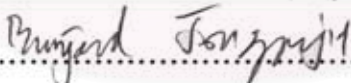
Field of Study   Chemical Engineering

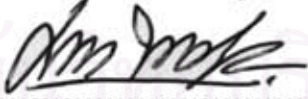Thesis Advisor   Assistant Professor Bunjerd Jongsomjit, Ph.D.

Accepted by the Faculty of Engineering, Chulalongkorn University in Partial Fulfillment of the Requirements for the Master's Degree
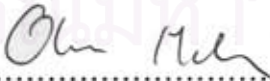
....................................Dean of the Faculty of Engineering

(Associate Professor Boonsom Lerdhirunwong, Dr.Ing.)

THESIS COMMITTEE

.... Chairman

(Professor Piyasan Praserthdam, Dr.Ing.)

.... Thesis Advisor

(Assistant Professor Bunjerd Jongsomjit, Ph.D.)

.... Member

(Associate Professor ML. Supakanok Thongyai, Ph.D.)

.... External Member

(Assistant Professor Okorn Mekasuwandamrong, Ph.D.)

สุภาวรรณ ศุภาณิชย์มงคล : ผลของความบกพร่องภายในและพื้นผิวของตัวรองรับไท
เทเนียที่มีต่อคุณลักษณะและสมบัติการเป็นตัวเร่งปฏิกิริยาของตัวเร่งปฏิกิริยาโคบอลต์บน
ตัวรองรับไทเทเนียด้วยปฏิกิริยาเมทาเนชัน (EFFECTS OF BULK AND SURFACE
DEFECTS OF TiO₂ SUPPORT ON THE PHYSICO-CHEMICAL
PROPERTIES OF Co/TiO₂ CATALYST VIA METHANATION) อ. ที่ปรึกษา :
ผศ. ดร. บรรเจิด จงสมจิตร, 77 หน้า

วิทยานิพนธ์นี้ ศึกษาถึงผลของความบกพร่องภายในผลึกและความบกพร่องบนพื้นผิวของ
ผลึกบนตัวรองรับไทเทเนียซึ่งเตรียมโดยวิธีโซลเจลที่มีต่อตัวเร่งปฏิกิริยาโคบอลต์ ด้วยวิธีฝังเคลือบ
โคบอลต์ลงบนตัวรองรับไทเทเนียซึ่งมีความบกพร่องภายในผลึกและบนความบกพร่องบนพื้นผิว
ผลึกต่างๆกัน โดยการเตรียมตัวรองรับไทเทเนียนั้นเตรียมจากงานก่อนหน้านี้ที่ผ่านมา จากนั้นนำ
ตัวเร่งปฏิกิริยาโคบอลต์บนตัวรองรับไทเทเนียไปตรวจสอบคุณลักษณะ โดยใช้การดูดซับทาง
กายภาพด้วยไนโตรเจน การกระเจิงรังสีเอ็กซ์ การส่องผ่านด้วยกล้องจุลทรรศน์อิเล็กตรอน การ
รีดักชันแบบโปรแกรมอุณหภูมิและการดูดซับด้วยไฮโดรเจนและศึกษาในปฏิกิริยาเมทาเนชัน ซึ่ง
พบว่าจะมีปริมาณของทั้งความบกพร่องภายในและบนพื้นผิวของผลึกไทเทเนียดีที่สุดหรือสมดุล
ที่สุดที่จะส่งผลให้ค่าการดูดซับด้วยไฮโดรเจนสูงที่สุด อุณหภูมิที่ใช้ในการรีดักชันต่ำที่สุดหรือ
สามารถรีดิวซ์จากโคบอลต์ออกไซด์ให้กลายเป็นโคบอลต์ซีโร่ที่เป็นแอคทีฟไซค์ได้ง่าย และยังทำ
ให้เปอร์เซ็นต์การเกิดมีเทนในปฏิกิริยามากที่สุด ซึ่งทั้งหมดนี้เป็นผลมาจากการฝังเคลือบโคบอลต์
ลงบนตัวรองรับไทเทเนียที่มีความบกพร่องภายในและความบกพร่องบนพื้นผิวผลึกที่ต่างกันซึ่งจะ
ส่งผลให้มีคุณสมบัติเอสเอ็มเอสไอต่างกันออกไป โดยคุณสมบัตินี้จะส่งผลต่อตัวเร่งปฏิกิริยา
โคบอลต์ให้มีคุณลักษณะและความสามารถในการทำปฏิกิริยาต่างกันออกไป

ภาควิชา.............วิศวกรรมเคมี...........	ลายมือชื่อนิสิต...............................		
สาขาวิชา...........วิศวกรรมเคมี...........	ลายมือชื่ออาจารย์ที่ปรึกษา...............		
ปีการศึกษา..........2550....................			

##4970653221: MAJOR CHEMICAL ENGINEERING

KEY WORD: COBALT/ TITANIA/ COBALT CATALYST/ BULK DEFECT/ SURFACE DEFECT/ METHANATION/ SMSI

SUPAWAN SPAWANITCHMONGKOL: EFFECTS OF BULK AND SURFACE DEFECTS OF TiO_2 SUPPORT ON THE PHYSICO-CHEMICAL PROPERTIES OF Co/TiO_2 CATALYST VIA METHNATION. THESIS ADVISOR: ASST. PROF. BUNJERD JONGSOMJIT, Ph.D., 77 pp.

In this work, the effects of bulk and surface defects on TiO_2 supports prepared by the sol-gel method were investigated over Co/TiO_2 catalyst. The 20%wt of cobalt were impregnated onto TiO_2 having different amounts of bulk and surface defects, which were prepared from the sol-gel method by controlling the water:alkoxide molar ratios during sol-gel synthesis. The Co/TiO_2 catalysts were characterized with different techniques including XRD, N_2-physisorption, SEM, TEM, H_2-chemisorption, temperature-programmed reduction (TPR). It showed that the optimum amount of bulk and surface defects can result in high total H_2 chemisorption, high reducibility, low reduction temperature, and consequently high conversion for methanation of the Co/TiO_2 catalyst. This was attributed to changes in the SMSI property superimposed with the interaction between cobalt and TiO_2 support caused by impregnate cobalt onto different bulk and surface defects on TiO_2.

Department......Chemical Engineering... Student's signature...Supawan Supawanitchmongk

Field of study...Chemical Engineering... Advisor's signature...Bunjerd Jongsi...

Academic year.....2007.....................

ACKNOWLEDGEMENTS

CONTENTS

LIST OF TABLES

LIST OF FIGURES

LISTS OF SCHEMES

CHAPTER I

INTRODUCTION

It has been known that the supported cobalt (Co) catalysts are used for carbon monoxide (CO) hydrogenation or Fischer-Tropch synthesis (FTS) because it can change carbon monoxide (CO) to valuable organic compound and have high activities and high selectivity to linear long chain hydrocarbons. They also have low activities for the competitive water-gas shift (WGS) reaction [1]. Three main factors controlling Co activity in FTS are (i) cobalt dispersion on support, (ii) reduction behavior, and (ii) Co-support compound formation (Co-SCF) [2,3]. However, the interaction between cobalt and support plays the important role to control all of these factors [4]. Normally, this interaction between cobalt and support depends on the nature of precursor, support, and also the method for synthesizing supported catalyst [4]. In this study, the $Co(NO_3)_2.6H_2O$ was used as the cobalt precursor and solvent for impregnation of cobalt onto the support.

The better way to find out the effect of metal-support interaction on three main factors and consequently on the catalytic activity is the use of the strong-metal support interaction (SMSI) catalyst for studying such as Co/TiO_2 system, which its characteristics and catalytic properties depend on the properties of TiO_2 support [1]. The surface defect is one of the crucial factors because the properties of the TiO_2 are often dependent on a nature and density of the surface defect sites [5]. For the nature of surface defect, Henrich and Kurtz [6] have shown that the dominant defect on the TiO_2 surface is oxygen vacancies site (Ti^{3+}). Our previous work found that an increase of surface defect (Ti^{3+}) on TiO_2 support can enhance the cobalt dispersion, reduction behavior, and consequently the activity of FTS of Co/TiO_2 catalyst [7,8]. However, surface defect is not the only factor controlling the characteristic and catalytic properties of TiO_2, but the bulk defect is also considered [9]. It has been known that there are many types of bulk defect and being no obvious to identify them [10]. However, high amount of bulk defect leads TiO_2 to have a low crystallinity, which is monitored by means of XRD [11,12]. As mentioned above, although the bulk defect also plays the important role controlling the TiO_2 properties, the effect of bulk defect

of TiO$_2$ support has not been investigated coinciding with surface defect (Ti^{3+}). Therefore, this work engages to study the effect of bulk defect coinciding with surface defect of TiO$_2$ support on the characteristics and catalytic properties of Co/ TiO$_2$ catalyst.

To control the bulk and surface defects of TiO$_2$ support at the same time, our previous work [9] was achieved the way to control both defects by varying the water:alkoxide molar ratios used during sol-gel synthesized TiO$_2$ nanocrystal [13]. After loading cobalt onto the TiO$_2$ support having different amounts of bulk and surface defects, the Co/TiO$_2$ catalysts were characterized using N$_2$ physisorption, temperature programmed reduction (TPR), hydrogen chemisorption, scanning electron microscopy (SEM), and transmission electron spectroscopy (TEM). The carbon monoxide (CO) hydrogenation under methanation was performed to determine the catalytic activity of different Co/TiO$_2$ catalysts.

The study was scoped as follows:

1. Preparation of the bulk and surface defects on TiO$_2$ supports via sol-gel method (water:alkoxide molar ratio in the range of 4-165).
2. Characterization of the surface and bulk defect on TiO$_2$ supports by using X-ray diffraction (XRD), N$_2$ physisorption, electron spin resonance spectroscopy (ESR), and CO$_2$-temperature programmed desorption (CO$_2$-TPD).
3. Preparation of supported Co catalyst on the defective TiO$_2$ supports (20 wt% Co) using the incipient wetness impregnation method.
4. Characterization of the catalyst samples using, X-ray diffraction (XRD), N$_2$ physisorption, hydrogen chemisorption, scanning electron microscopy (SEM), transmission electron spectroscopy (TEM) and temperature programmed reduction (TPR).
5. Investigation of the catalytic activity of Co/TiO$_2$ catalyst in the hydrogenation of carbon monoxide (CO) at 220°C and 1 atm and a H$_2$/CO ratio of 10.

CHAPTER II

LITERATURE REVIEWS

As known that Co/TiO_2 catalyst is considered to have strong metal support interaction [14,15] and shows high activities in CO hydrogenation. Therefore, This chapter reviews the work about TiO_2 properties such as, bulk and surface defects that had effects to improve Co/TiO_2 catalys. Moreover, several studies about the effect of cobalt precursors on supported cobalt catalyst.

2.1 Defect (Ti^{3+}) controlling on TiO_2

2.1.1 Bulk defect controlling

Defect structure of TiO_2 in bulk is difficult to control and being detected (it can detect only Rietveld analysis from XRD) because it has several types of defect. However, there are only few works which discussed in this topic such as Jung et al. [10], Wang et al. [16,17]. They concluded that bulk defect (which is detected by using Rietveld analysis) decreased with increasing annealing temperature. Moreover, these bulk defects increased with increasing the amount of metal doping.

2.1.2 Surface defect controlling

There are a few types of surface defect on TiO_2. However, Henrich and Kurtz have shown that the dominant defects on TiO_2 surfaces are only oxygen anion vacancies [6]. Wallace et al. [18] reported that surface defect (Ti^{3+}) plays the significant roles enhancing the dispersion and stability of supported gold cluster via the strong interaction (SMSI) between the defect site and metal cluster. Thus, it demonstrates that the creation of surface defect (Ti^{3+}) on anatase is necessary for improving its properties for many applications. Suriye et al. [19] studied create the surface defect (Ti^{3+}) on TiO_2 and compared to the common methods which must prepare the crystalline TiO_2 in the first step prior, and then create the surface defect in the second step. In this work, the surface defect creation was performed in the first step coinciding with the crystalline TiO_2 preparation using the sol–gel method. The

creation was performed by varying the amounts of oxygen fed during calcination. the surface defect (Ti^{3+}) substantially increased with the amount of oxygen fed. Moreover, the samples resulting from calcination were used as photocatalysts for ethylene decomposition. He found that a new method for surface defect creation coinciding with crystalline TiO_2 preparation in the first step was performed by changing the amounts of oxygen fed during the calcination process. Using CO_2-TPD and ESR, it was found that the surface defect density (Ti^{3+}) could be increased by increasing the amount of oxygen fed. Also, the increased Ti^{3+} amounts did not result from the reduction of Ti^{4+} to Ti^{3+} due to low calcination temperature used in the absence of hydrogen. The removal of the surface hydroxyl group when exposed to increased oxygen concentration accounts for the formation of the surface defect (Ti^{3+}).

2.1.3 Surface defect coinciding bulk defect

Suriye et. al. [9] studied the results on the surface defect controlling in the first step coinciding with the preparation of TiO_2 in anatase phase via sol-gel synthesis were reported. In this work, the surface defect was controlled by varying the calcination atmosphere. The surface defect controlling by varying the water:alkoxide molar ratio has been successfully created at mild temperature coincinding with the preparation of crystalline TiO_2 in anatase phase. No phase transformation and significant surface area loss on the resulting anatase after surface defect creation

2.2 Co-support compound formation

B. jongsomjit et. al. [3] research to showed dependence of crystalline phases in titania on the catalytic properties of Co/TiO_2 catalysts during CO hydrogenation. A comparative study of anatase TiO_2- and rultile-anatase coupled TiO_2-supported Co catalysts was conducted. It was found that the presence of rutile phase (19 mol%) in titania resulted in a significant increase in the catalytic activity during CO hydrogenation. It was proposed that the role of rutile phase was to increase the stability of the support. The impact of water vapor produced during reduction on the formation of cobalt species strongly interacted with the support was probably

inhibited by the presence of rutile phase in titania leading to a decrease in the reducibility loss during reduction and study has shown the dependence of crystalline phases in titania on the catalytic properties during CO hydrogenation of Co/TiO_2 catalysts. The presence of rutile phase (19 mol%) in titania resulted in significant increases in the catalytic activities during CO hydrogenation. This is mostly due to an increase in stability of the titania support with the presence of rutile phase. It was found that the presence of rutile phase enhanced the stability of the titania support and also catalysts themselves leading to lesser degrees of a loss in reducibility after hydrothermal treatments during reduction of catalysts. It was proposed that the presence of rutile phase in titania stabilized the catalysts probably due to two reasons: (i) block the formation of Co species strongly interacted with the titania support or Co-SCF; and (ii) inhibition of the impact of water vapor produced during reduction.

2.3 Effect of surface defect on metal-support interaction on Co/TiO_2 catalyst

The interaction between a support and a metal oxide (catalyst) precursor is an important factor used to determine the dispersion of a metal catalyst and hence the behavior of a catalyst as well [2]. In fact, the synthesis of highly dispersed cobalt catalysts requires the initial formation of very small Co_3O_4 crystallites. It was reported that the formation of small oxide clusters needs strong interactions between the support and the cobalt precursor. However, too strong interaction would suppress reduction of these CoO_x clusters [20] resulting in low reducibilities. Moreover, strong interaction between Co and TiO_2 can produce the suboxide at interface that is more resistant to reduction than the other supports. There also are many reports showing the effect of surface site as a surface defect on the interaction of metal and oxide, as summarized by Diebold [21]. It has been known that the bond energy for anchoring of the metal is larger at the surface defect site than at the perfect sites [22]. This is because the surface defect sites have one lone pair electron at *d* orbital resulted in the higher reactive with the metal and oxide loading [21]. Based on this bond energy, Wallace et al. summarized the role of Ti^{3+} site on Au cluster nucleation, growth, and stability on Ti^{3+} site of TiO_2 support [18]. It showed that an increase of Ti^{3+} site strongly decreases the rate of Au cluster migration during high temperature condition due to the strongly bonding between Ti^{3+} site and Au cluster. Also the reports showing the strong bonding between Gr. VIII metals and Ti^{3+} have been done by

many researchers [21,23,24]. Moreover, Suriye et.al [7] investigated the effect of the defect structure referred to as Ti^{3+} present in titania support of supported titania on characteristics and activity of the Co/TiO_2 catalyst. Titania supports were prepared by sol-gel and then calcined under N_2 plus increasing the amount of O_2 to change the surface defect concentration. The surface defect of titania support was increased by increasing the oxygen percent in feed during the calcination process.. It was found that dispersion of cobalt and reducibility increased with the amount of surface defect present. This work showed the impact of Ti^{3+} present in titania support on characteristics and catalytic properties of Co/TiO_2 catalysts on methanation. The presence of Ti^{3+} in titania support increased with an increasing amount of $\%O_2$ in feed during the calcination process. The amount of Ti^{3+} present in titania support apparently affected the characteristics of the Co/TiO_2 catalyst. Cobalt dispersion increased with the amount of Ti^{3+} present in titania because of enhancing the strong interaction degree. the oxygen vacancy site was enhanced with the presence of Ti3+ in titania support. The reduction behavior of the Co/TiO_2 catalyst also changed due to Ti^{3+} present in titania support. It showed that high reducibility occurred when more Ti^{3+} was present in supports. The various Co/TiO_2 samples were tested for their activities for the methanation. The unchanged CH_4 selectivity of the Co/TiO_2 samples were observed. It can be concluded that strong interaction arising from the presence of Ti^{3+} in titania support can enhance conversion of CO on methanation without changing CH_4 selectivity. Suriye et. al [8] study the effect of surface sites (as Ti^{4+} and $Ti^{3+)}$ of TiO_2 support on the formation of the cobalt-support compound

on Co/TiO_2 catalyst. A 20% cobalt was prepared on each TiO_2 support having the different Ti^{4+}/Ti^{3+} ratios covering on the surface It can be concluded that the non-reducible compound as a Co-SCF preferred to form on the Co/TiO_2 catalyst when the most proportional site of surface TiO_2 became $Ti^{4+.}$ This is because the migration of cobalt cluster, which plays the significant role for creating Co-SCF can be promoted by the increasing of Ti^{4+} sites resulting in the decrease of cobalt dispersion. the effect of surface species (as a Ti^{4+} and Ti^{3+} on TiO_2 support) on the cobalt-support compound formation (Co-SCF) was investigated on the Co/TiO_2 catalyst. It revealed that the Co-SCF preferred to form on Co/TiO_2 catalyst when the most proportion surface site of TiO_2 support became $Ti^{4+.}$ Based on ESR spectra, it was demonstrated that the Co-SCF had a simple chemical form as a $Co^0(H_xTiO_y)$. This compound reached to be a higher non-uniform structure when the number of Ti^{4+} on TiO_2 surface

increased. These are the promising knowledge that should be used to develop the characteristics of Co/TiO$_2$ catalyst especially the formation of Co-SCF. The number of Ti^{4+} should be decreased as much as possible to prevent the formation of such the compound. It might be done treating the TiO$_2$ surface prior to preparing the Co/TiO$_2$ catalyst.

CHAPTER III

THEORY

3.1 Defect structure of crystal material

Defects can be broadly divided into two groups: stoichiometric defects in which the crystal composition is unchanged on introducing the defects and non-stoichiometric defects, which are a consequence of a change in crystal composition. Some phenomena cannot be explained without invoking the presence of defects. These include:

1. Understanding the forces required fracturing a crystal. If one simply calculated the force required to separate two layers of atoms in a crystal, the result would come out to be much larger that the actual force required fracturing a solid. It therefore appears as if a crystal breaks in stages, with each stage requiring a rather smaller force.

2. The ability of a crystal to deform irreversibly under stress. The primary example is called slip. Where application of a stress acts as a shear stress on particular crystal planes that appear to slide over each other.

3. The origin of color in many materials that would otherwise be transparent. A well-known example is the red color of ruby, Al_2O_3, which is caused by Cr^{3+} impurities on the Al sites

4. The presence of a small but non-zero electrical conductivity in insulators, these are caused by the motion of charged ions as in a salt solution. Ionic conductivity is much higher in materials that contain vacant sites as defects.

5. The ability of atoms to diffuse within a solid, such as the diffusion of carbon atoms in iron. The processes are related to those that allow electrical conductivity.

6. Crystal growth, which often appears to proceed through a process that, involves the formation of a spiral defect.

The presence of defects can be exploited in applications, and in other cases the presence of defects causes technological problems, and both mean that it is important to understand the behavior of defects. Two such defects particular importance is the Frenkel and Schottky defects. Only point defect that concerns our work thus large-scale imperfections will not mentioned in details. The details of point defects are following

3.1.1 Vacancies: Schottky defects

Consider the simplest crystal defect, namely that of an atomic site becoming vacant, with the missing atom migrating to the crystal surface. This process will be energetically unfavorable, costing the system a change in energy.

The simple case of a vacant site is called a Schottky defect. In order to maintain a neutral charge distribution across a local length scale, it is common for both positive and negative vacant sites to be produced in thermal equilibrium and to be evenly distributed throughout the sample. This is represented in Figure 3.1.
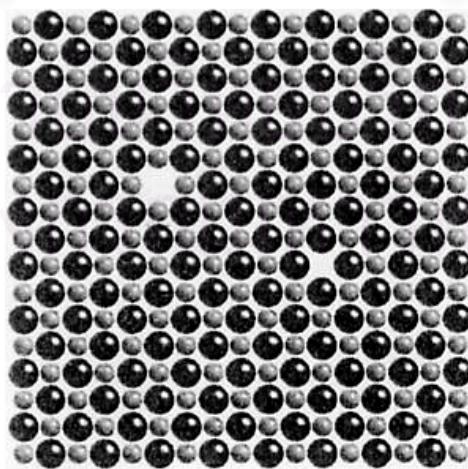
Figure 3.1 Cation and anion charge-balanced Shottky defects in NaCl.

3.1.2 Interstitial defects: Frenkel defects

In crystals that not pack with high efficiency, it is possible for atoms to occupy sites that are normally vacant, called interstitial sites. A Frenkel defect occurs when at atom leaves its normal site to create a vacancy, and is then displaced into one of the interstitial sites. This process is illustrated in Figure 3.2.
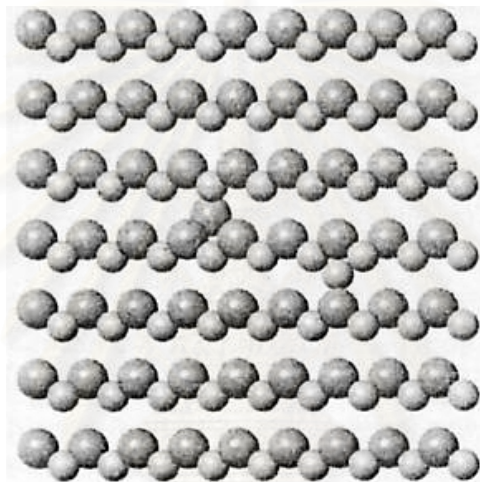
Figure 3.2 Pair of charge-balanced Frenkel defects in AgI.

3.1.3 Coupled charge substitutions and vacancies

The vacancies that mentioned above occur as equilibrium processes. Other point defects can be produced as non-equilibrium structures through the process of crystal growth. A common defect is the substitution of a different type of atom, usually one of similar charge. For example, NaCl can contain K^+ defects substituting for the cation sites, or F^- substituting on the anion sites. A substitution of a different charged cation will require production of a compensating charge defect. For example, substituting a Ca^{2+} cation in NaCl will require the formation of a charge-compensating cation vacancy. This structure is illustrated in Figure 3.3.
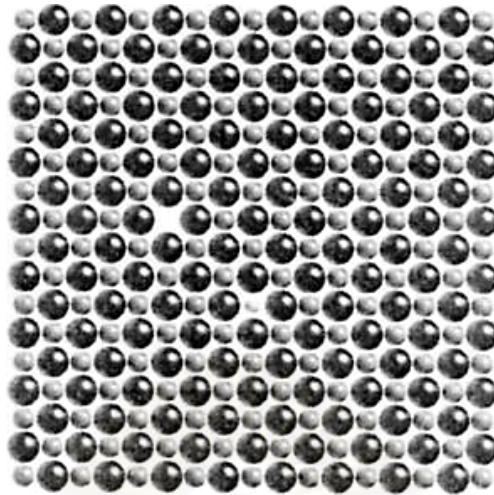
Figure 3.3 Substitution of a Ca^{2+} cation for a Na$^+$ cation in NaCl, accompanied by the formation of a vacant cation site in order to maintain charge neutrality.

3.1.4 Color centers

The charge substitutions that have considered have been restricted to ions. It is also possible for electrons to occupy vacant anion sites in order to maintain charge neutrality. The electron forms its own energy bands. The color center is able to absorb electromagnetic radiation in the visible spectrum, and this gives color to what would otherwise be a transparent crystal. As a result, the presence of the color center can be detected in an optical absorption experiment.

3.2 Surface defects

There is a sense in which the surface itself with it's coordinatively atoms it the most numerous type of defect. The bulk of the experimental results, spectroscopic or otherwise, necessarily relate to adsorption on the more numerous and expected sites on oxide surface, such as coordinatively unsaturated cations or anions, hydroxyls, acid-base pair, etc. However the most active sites will be connected with defects in the normal surface, which have unusual geometrical and/or local chemical compositional features. These may be present in concentrations that are one or two

orders of magnitude less than those of the regular sites and their experimental detection can be correspondingly different.

In general, the majority of the experimental phenomena discussed above were connected with adsorption on the more numerous and expected sites on the oxide surface (coordinatively unsaturated cations, anions, hydroxyls, and their pair). However, the appearance of the most active surface centers suggests a connection with defects in the solid. The other factors influencing the properties of the real oxide surfaces are: (i) the presence of different lattice defects in the surface layer, and (ii) their chemical composition, which in many cases, may differ from that in the bulk.

In spite of the fact that the concentration of the defect centers on the surface is one or even two orders of magnitude less than the concentration of regular active sites, their reactivities are very often higher. This is why such defect centers can participate in the reaction.

The presence of the so-called dangling bonds (unsaturated valencies) at the surface creates electron energy states, usually named intrinsic states, which are present even in the case of pure and strictly stoichiometric surface. Additional structural defects on the surface which may be or may be not associated with adsorbed impurities, said to create extrinsic surface states.

The role of intrinsic defects in the activation of adsorbed molecules has not yet been elucidated. The physics of such defects is also still in development. In contrast, the influence of extrinsic defects on chemisorption and catalysis has been the object of many investigations.

Crystal with periodical arrangements of all of their structural elements cannot exist and real crystals show the presence of various imperfections described as defects. Those atoms into other sites or interstitial positions may due to (i) the displacement of atoms from the lattice sites normally occupy them, (ii) the presence of some vacant sites, or (iii) the displacement of part of a crystal with respect to another part along a crystal plane, etc. These defects are usually classified according to their dimensions into point defects (vacancies interstitial or foreign atoms), linear

defects (dislocations) and spatial defects such as pores of foreign inclusion. For example, besides being a strong base, the highly dehydroxylated MgO surface is a good reducing agent. The reducing sites are apparently defects, possibly surface cation vacancies: the dissociative chemisorption of Bronsted acids blocks the reactivity of the reducing sites.

Investigation of small-surface-area bulk alkali earth-metal oxides, including MgO, e.g. as single crystal, show that their photoluminescence is caused by defects in the crystalline lattice, namely by the F^+ and $F^{\bullet}$ centers, i.e. the oxygen vacancies have captured one or two electrons, respectively. Such centers can be easily detected directly by EPR and/or by UV-Vis spectroscopic studies of the adsorption of molecules that easily form cation or anion radicals. Detailed analysis of such spectra obtained by using molecules which different but known values of ionization potential (IP) or electron affinity, allows us to obtain information about such an adsorption center, for example, on the basis of data on the transition to the radical state, and so to make a conclusion about its redox properties.

The main method used to investigate such centers is electron paramagnetic resonance (EPR) spectroscopy. It should be remembered that the formation of radicals could proceed on the surface of practically all oxide systems, when easily ionizable adsorbates which are able to cause the formation of both main and side-reaction products, are used.

A connection with the problem of defect sites, studies of mechanically activated oxide systems seem to be very interesting and useful. It is well known that mechanical activation (by grinding) affects an increase in the number of defects formed upon mechanical activation.

Mechanical treatment is an effective method for creating defects in solids. Various mechanical activation effects are related to the formation of such defects and their subsequent chemical transformations. Some of these defects are free radicals, for example in the case of SiO_2 $(=Si-O-)_3Si^{\bullet}$ and $(=Si-O-)_3SiO^{\bullet}$. A new type of natural defect, namely silanone (Si=O) groups was identified on the surface of mechanically

activated SiO_2. A study was carried out by using their thermal stabilities, optical properties (a characteristic absorption band was found with a maximum at 5.3 Ev) and alcination, relative to simple molecules, such as CO_2 and N_2O, and radicls, such as H, D and CH_3. Studies of the IR and Raman spectra of the oxides MgO, Cr_2O_3, MoO_3, Co_3O_4 and CuO in the regions of the cutoff vibrations allowed identification of sample amorphization during mechanical activation ans also the decrease in the coordination number of both cations and anions as compared with nonactivated oxides. The latter bring to increases in the reactivities. According to IR spectra of adsorbed CO in the case of CuO and Co_3O_4, the reduction of Cu^{2+} to Cu^+ and Co^{3+} to Co^{2+} cations was observed during mechanical activation.

In the diffuse reflectance electron spectroscopy (DRES) spectra of MoO_3, the valence-to-conduction band transition exhibited a considerable blue shift with decreasing particle size. Excitonic absorptions observed in these spectra are also affected by the smaller particle size and by the altered crystallite surface. An increasing intensity of the bands was observed, and a linear dependence between the position of the band attributed to polaron conductance and the logarithm of the carrier concentration per Mo atom was obtained, both of these fact reveals that a sub-stoichimetric MoO_{3-x} species was formed upon mechanical treatment. According to the ESR data, both milled and non-milled MoO_3 samples contained Mo^{5+} centers interacting with OH groups in close vicinity, but their concentration was much smaller in the case of non-milled MoO_3. The main portion of these Mo^{5+} ions had C_{2v} or C_{4v} symmetry. These latter ions appear to result from the mechanical activation process and are suggested to be the precursors of a crystallographic shear structure. Exposure to O_2 reveals that all of these Mo^{5+} sites are located in the bulk and not necessarily on the surface, whereas free electrons are present at the surface. The high surface sensitivity of the IR technique when using adsorbed probe molecules revealed the formation of coordinatively unsaturated Mo^{4+} surface states in MoO_3 which was mechanically activated.

3.3 Titanium (IV) oxide

Titanium (IV) oxide occurs naturally in three crystalline forms: anatase, which tends to be more stable at low temperature, brookite, which is usually found only in minerals, and rutile, which tends to be more stable at higher temperatures and thus is sometimes found in igneous rock. These crystals are substantially pure titanium (IV) oxide but usually amounts of impurities, e.g., iron, chromium, or vanadium, which darken them. A summary of the crystallographic properties of the three varieties is given in Table 3.1.

Although anatase and rutile are both tetragonal, they are not isomorphous (Figure 3.4). Anatase occurs usually in near-regular octahedral, and rutile forms slender prismatic crystal, which are frequently twinned. Rutile is the thermally stable form and is one of the two most important ores of titanium.

The three allotropic forms of titanium (IV) oxide have been prepared artificially but only rutile, the thermally stable form, has been obtained in the form of transparent large single crystal. The transformation form anatase to rutile is accompanied by the evolution of ca. 12.6 Kj/mol (3.01 kcal/mol), but the rate of transformation is greatly affected by temperature and by the presence of other substance which may either catalyze of inhibit the reaction. The lowest temperature at which conversion of anatase to rutile takes place at a measurable rate is ca. 700°C, but this is not a transition temperature. The change is not reversible; ΔG for the change from anatase to rutile is always negative.
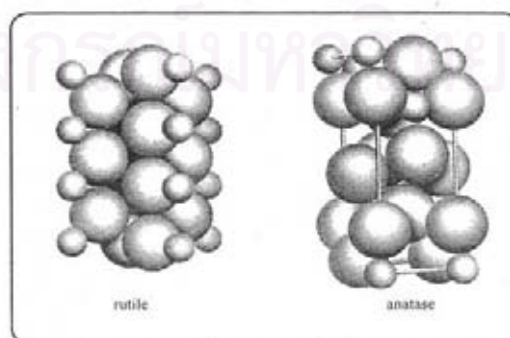
Figure 3.4 Crystal structure of TiO_2. (Fujishima *et al.*,1999)

Brookite has been produced by heating amorphous titanium (IV) oxide, prepared from alkyl titanates of sodium titanate with sodium or potassium hydroxide in an autoclave at 200 to 600°C for several days. The important commercial forms of titanium (IV) oxide are anatase and rutile, and these can readily be distinguished by X-ray diffraction spectrometry.

Since both anatase and rutile are tetragonal, they are both anisotropic, and their physical properties, e.g. refractive index, vary according to the direction relative to the crystal axes. In most applications of these substances, the distinction between crystallographic directions is lost because of the random orientation of large numbers of small particles, and it is mean value of the property that is significant.

Table 3.1 Crystallographic properties of anatase, brookite, and rutile.

Properties	Anatase	Brookite	Rutile
Crystal structure	Tetragonal	Orthorhombic	Tetragonal
Optical	Uniaxial, negative	Biaxial, positive	Uniaxial, negative
Density, g/cm^3	3.9	4.0	4.23
Harness, Mohs scale	$5^1/_2 - 6$	$5^1/_2 - 6$	$7 - 7^1/_2$
Unit cell	$D_4a^{19}.4TiO_2$	$D_2h^{15}.8TiO_2$	$D_4h^{12}.3TiO_2$
Dimension, nm			
a	0.3758	0.9166	0.4584
b		0.5436	
c	0.9514	0.5135	2.953

Measurement of physical properties, in which the crystallographic directions are taken into account, may be made of both natural and synthetic rutile, natural anatase crystals, and natural brookite crystals. Measurements of the refractive index of titanium (IV) oxide must be made by using a crystal that is suitably orientated with respect to the crystallographic axis as a prism in a spectrometer. Crystals of suitable size of all three modifications occur naturally and have been studied. However, rutile

is the only form that can be obtained in large artificial crystals from melts. The refractive index of rutile is 2.75. The dielectric constant of rutile varies with direction in the crystal and with any variation from the stoichiometric formula, TiO_2; an average value for rutile in powder from is 114. The dielectric constant of anatase powder is 48.

Titanium (IV) oxide is thermally stable (mp 1855°C) and very resistant to chemical attack. When it is heated strongly under vacuum, there is a slight loss of oxygen corresponding to a change in composition to $TiO_{1.97}$. The product is dark blue but reverts to the original white color when it is heated in air.

3.4 Cobalt (Young 1960; Othmer, 1991)

3.4.1 General

Cobalt, a transition series metallic element having atomic number 27, is similar to silver in appearance. Cobalt and cobalt compounds have expended from use colorants in glasses and ground coat frits for pottery to drying agents in paints and lacquers, animal and human nutrients, electroplating materials, high temperature alloys, hard facing alloys, high speed tools, magnetic alloys, alloys used for prosthetics, and used in radiology. Cobalt is also as a catalyst for hydrocarbon refining from crude oil for the synthesis of heating fuel.

3.4.2 Physical Properties

The electronic structure of cobalt is [Ar] $3d^7 4s^2$. At room temperature the crystalline structure of the α (or ε) form, is close-packed hexagonal (cph) and lattice parameters are a = 0.2501 nm and c = 0.4066 nm. Above approximately 417°C, a face-centered cubic (fcc) allotrope, the γ (or β) form, having a lattice parameter a = 0.3544 nm, becomes the stable crystalline form. Physical properties of cobalt are listed in Table 3.2.

The scale formed on unalloyed cobalt during exposure to air or oxygen at high temperature is double-layered. In the range of 300 to 900°C, the scale consists of a thin layer of mixed cobalt oxide, Co_3O_4, on the outside and cobalt (II) oxide, CoO, layer next to metal. Cobalt (III) oxide, Co_2O_3, may be formed at temperatures below 300 $^{\circ}$C. Above 900°C, Co_3O_4 decomposes and both layers, although of different appearance, are composed of CoO only. Scales formed below 600°C and above 750°C appear to be stable to cracking on cooling, whereas those produced at 600-750°C crack and flake off the surface.

Cobalt forms numerous compounds and complexes of industrial importance. Cobalt, atomic weight 58.933, is one of the three members of the first transition series of Group 9 (VIIIB). There are thirteen know isotopes, but only three are significant: ^{59}Co is the only stable and naturally occurring isotope; ^{60}Co has a half-life of 5.3 years and is a common source of γ-radioactivity; and ^{57}Co has a 270-d half-life and provides the γ-source for Mössbauer spectroscopy.

Cobalt exists in the +2 or +3 valance states for the major of its compounds and complexes. A multitude of complexes of the cobalt (III) ion exists, but few stable simple salt are known. Octahedral stereochemistries are the most common for cobalt (II) ion as well as for cobalt (III). Cobalt (II) forms numerous simple compounds and complexes, most of which are octahedral or tetrahedral in nature; cobalt (II) forms more tetrahedral complex than other transition-metal ions. Because of the small stability difference between octahedral and tetrahedral complexes of cobalt (II), both can be found equilibrium for a number of complexes. Typically, octahedral cobalt (II) salts and complexes are pink to brownish red; most of the tetrahedral Co (II) species are blue.

Table 3.2 Physical properties of cobalt (Othmer, 1991)

Property	Value	
atomic number	27	
atomic weight	58.93	
transformation temperature, ^{o}C	417	
heat of transformation, J/g[a]	251	
melting point, ^{o}C	1493	
latent heat of fusion, ΔH_{fus} J/g[a]	395	
boiling point, , ^{o}C	3100	
latent heat of vaporization at bp, ΔH_{vap} kJ/g[a]	6276	
specific heat, J/(g^{o}C)[a]		
15-100°C	0.442	
molten metal	0.560	
coefficient of thermalexpansion, ^{o}C^{-1}		
cph at room temperature	12.5	
fcc at 417°C	14.2	
thermal conductivity at 25 ^{o}C, W/(m·K)	69.16	
thermal neutron absorption, Bohr atom	34.8	
resistivity, at 20 ^{o}C[b], 10^{-8} Ω·m	6.24	
Curie temperature, ^{o}C	1121	
saturation induction, $4\pi I_s$, T[c]	1.870	
permeability, μ		
initial	68	
max	245	
residual induction, T[c]	0.490	
coercive force, A/m	708	
Young's modulus, Gpa[c]	211	
Hardness[f], diamond pyramid, of %Co	99.9	99.98[e]

Table 3.2 Physical properties of cobalt (Othmer, 1991)

Property	Value	
At 20 °C	225	253
At 300 °C	141	145
At 600 °C	62	43
At 900 °C	22	17

strength of 99.99 % cobalt, MPa[g]	as cast	annealed	sintered
tensile	237	588	679
tensile yield	138	193	302
compressive	841	808	
compressive yield	291	387	

[a] To convert J to cal, divided by 4.184.

[b] conductivity = 27.6 % of International Annealed Copper Standard.

[c] To convert T to gauss, multiply by 10^4.

[d] To convert GPa to psi , multiply by 145,000.

[e] Zone refined.

[f] Vickers.

[g] To convert MPa to psi , multiply by 145.

3.4.3 Cobalt Oxides

Cobalt has three well-known oxides:Cobalt (II) oxide, CoO, is an olive green, cubic crystalline material. Cobalt (II) oxide is the final product formed when the carbonate or the other oxides are calcined to a sufficiently high temperature, preferably in a neutral or slightly reducing atmosphere. Pure cobalt (II) oxide is a difficult substance to prepare, since it readily takes up oxygen even at room temperature to re-form a higher oxide. Above about 850°C, cobalt (II) oxide form is the stable oxide. The product of commerce is usually dark gray and contains 75-78 wt % cobalt. Cobalt (II) oxide is soluble in water, ammonia solution, and organic

solvents, but dissolves in strong mineral acids. It is used in glass decorating and coloring and is a precursor for the production of cobalt chemical.

Cobalt (III) oxide, Co_2O_3, is form when cobalt compounds are heated at a low temperature in the presence of an excess of air. Some authorities told that cobalt (III) oxide exists only in the hydrate form. The lower hydrate may be made as a black power by oxidizing neutral cobalt solutions with substances like sodium hypochlorite. Co_2O_3 or $Co_2O_3 . H_2O$ is completely converted to Co_3O_4 at temperatures above $265^{\circ}C$. Co_3O_4 will absorb oxygen in a sufficient quantity to correspond to the higher oxide Co_2O_3.

Cobalt oxide, Co_3O_4, is formed when cobalt compounds, such as the cabonate or the hydrated sesquioxide, are heated in air at temperatures above approximately $265^{\circ}C$ and not exceeding $800^{\circ}C$.

3.5 Co-based Catalysts

Supported cobalt (CO) catalysts are the preferred catalysts for the synthesis of heavy hydrocarbons from natural gas based syngas (CO and H_2) because of their high Fischer-Tropsch (FT) activity, high selectivity for linear hydrocarbons and low activity for the water-gas shift reaction. It is known that reduced cobalt metal, rather than its oxides or carbides, is the most active phase for CO hydrogenation in such catalysts. Investigations have been done to determine the nature of cobalt species on various supports such as alumina, silica, titania, magnesia, carbon, and zeolites. The influence of various types of cobalt precursors used was also investigated. It was found that the used of organic precursors such as CO (III) acetyl acetate resulting in an increase of CO conversion compared to that of cobalt nitrate.(Kraum and Baerns, 1999)

3.6 Fischer-Tropsch synthesis (FTS)

Fischer-Tropsch synthesis (FTS) that discovered by Fischer and Tropsch over 80 years ago, as an alternate process, can convert the synthesis gas (H_2/CO) derived from carbon sources such as coal, peat, biomass and natural gas, into hydrocarbons and oxygenates. During the past decades, FTS has been developed continuously by many researchers, although the rise and fall in research intensity on this process has been highly related to the demands for liquid fuels and relative economics. This synthesis is basically the reductive polymerization (oligomerization) of carbon monoxide by hydrogen to form organic products containing mainly hydrocarbons and some oxygenated products in lesser amounts.

By manipulation of the reaction conditions, the process may be designed to produce heavier saturated hydrocarbons or lower olefins or oxygenated hydrocarbons as we shall see in the following discussion.

Metals that have significant activity for Fischer-Tropsch synthesis include iron, cobalt, nickel and ruthenium. Iron has proved so far to be the best. It is superior to cobalt with respect to conversion rate, selectivity and flexibility. Nickel has disadvantage of producing appreciable amounts of methane. Ruthenium enhance the formation of high molecular weight alkanes and catalyzes polymerization to polymethane. Other group VIII metals are of low activity. Copper does not catalyze Fisher-Tropsch synthesis.

The catalyst is usually prepared by fusion or precipitation over a silica, alumina or kieselguhr support. Small amounts of promoters such as alkalu metal or copper salts are included in the catalytic mix. Copper is believe to facilitate the reduction of the catalyst, alkali metal salt, particularly K_2O_2 enhance activity and olefins selectivity. The support increased the surface area of the catalyst metal thus extremely increasing in dispersion.

Sulfur compounds generally poison the catalyst and they must be removed from the synthesis gas feed stream. However, partial sulfur poisoning may have favorable effects. Thus, it has been found that deliberate slight sulfur poisoning of the iron/manganese catalyst enhances selectivity to shot chain olefins.

Three main types of reactors are currently in use in the Fischer-Tropsch processes: Fixed-bed, fluidized-bed and slurry bed reactors. Fixed-bed reactors are usually tubular, each tube having 50 mm ID and 12 m length. A single reactor may contain as many as 2000 such tubes. Fluidized-bed reactors provide for better heat transfer and continuous regeneration of the catalyst. The catalyst used in fluidized-bed reactors must have high physical stability. SASOL (in Sought Africa), uses fluidized-bed reactors 46 m high, 230 cm in diameter with reaction temperature of 320-360ºC and pressure. In the slurry-bed reactors the feed gas is bubbled through a suspension of finely divided catalyst particles. It has the advantage of good temperature control thus providing greater flexibility of reaction conditions.

Each type of reactor is better suited for certain product composition. Fixed-bed reactors, for example, produce high boiling straight-chain hydrocarbons consisting, typically, of 33% gasoline hydrocarbons (C_5-C_{11}), 17% diesel and 40% heavy paraffins and higher waxes. The gasoline fraction is of low octane value and requires further treatment (isomerization or blending) before use. Fluidized-bed reactors are the best when lighter hydrocarbons are desired. A typical product composition is 72% lower molecular weight gasoline-range hydrocarbons rich in olefins and 14% oxygenated hydrocarbons. However, the product is low in diesel. Thus two or more different reactors may be operated in parallel to provide an integrated fuel plant.

The demands on selectivity of Fischer-Tropsch reactions are ever-increasing. In the earlier days of the process the concern was to improve selectivity with respect to better gasoline grade and/or diesel oil chemicals. With the realization of feasible route of converting synthesis gas to industrial intermediates, more stringent conditions are being imposed on the reaction parameters to make the process more selective.

Selectivity improvement is sought with respect to product properties such as chain length, chain branching, olefin content, alcohol content and methane content.

Reaction conditions that particularly eliminate or minimize carbon deposition are desirable. In order to achieve and improve product selectivity the optimization of the following reaction parameters has been investigated: reaction temperature and pressure, H_2/CO ratio, conversion, space velocity, amount and type of promoters, nature of the catalyst, size of catalyst particles and mode of its deposition, type of support, and type of reactor.

We have already seen examples of how the choice of the metal catalyst and support affects the product distribution. The effect of the choice of the reactor type on the nature of the reaction products has also been demonstrated.

Selectivity to olefins may be enhanced by addition of promoters such as K_2O, Ti, Mn or V. Selectivity of greater than 70% to C_2-C_4 olefins at high conversion rate has been achieved.

The search for selectivity to lower olefins by controlling the chain growth and inhibiting hydrogenation has been followed in three directions:

(a)   The use of highly dispersed catalyst either by improving the method of deposition or using special dispersing supports.

(b)   The use of bimetallic catalyst eg. With Mn/Fe ratio of 9:1 at 330 ºC up to 90% olefin selectivity has been achieved. However, the activity of the catalyst and its life-time are low.

(c)   The use of shape-selective catalyst.

Since the Fischer-Tropsch process was originally in intended for the production of hydrocarbons, little attention was paid in the early phases of the application of the process to the oxygenated products obtained as co-products. With the search for more economical sources of the oxygenated hydrocarbons, the possibility of tuning the Fischer-Tropsch process for the production such as oxygenates has been investigated. It has been found that with a nitrided iron catalyst, selectivity for alcohols may exceed 80%. A $Rh/Hg/SiO_2$ catalyst system gave 75% selectivity with respect to ethanol. The major side products are olefins.

The Fischer-Tropsch process may be defined as being the hydrogenative oligomerization of CO over heterogeneous catalyst to produce alkanes, alkenes oxygenated hydrocarbons and water. A complete mechanism must account for the formation of all products observed. The first attempt at eludicidating the mechanism of the process was made by the inventors of the process themselves, Fischer and Tropsch.

3.6.1 The surface carbide mechanism

Fischer and Tropsch apparently were trying to exolain the formation of alkanes and alkenes rather than introduce a mechanism for whole line of the products that could be formed from the process. They observed that hydrocarbon formation occurred with heterogeneous metal catalysts (Ni, Fe, Co, Ru) that tend to absorb CO dissociatievly to firm surface carbide species. Their mechanism consists of the following steps:

(i) Initiation:

$$M+CO \longrightarrow \overset{\overset{\textstyle O}{\overset{\textstyle |}{\overset{\textstyle C}{|}}}}{M} \overset{M}{\longrightarrow} \overset{\overset{\textstyle C}{|}\ \overset{\textstyle O}{|}}{M+M}$$

$$2M+H_2 \longrightarrow \overset{\overset{\textstyle H}{|}}{2M}$$

$$\overset{\overset{\textstyle H}{|}\ \overset{\textstyle C}{|}}{M\ +M} \longrightarrow \overset{\overset{\textstyle CH}{|}}{M+M} \longrightarrow \longrightarrow \overset{\overset{\textstyle CH_3}{|}}{M}$$
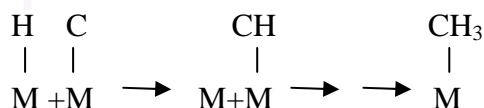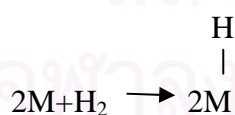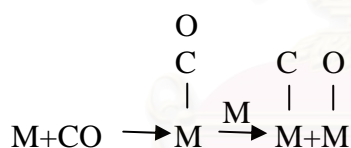
Note: M-X means species X chemisorbed on the metal surface atom M. The hyphen has no implication with respect to the strength of the M-X interaction

or the order of the bond. More recently it has been suggested, based spectroscopic evidence, that in order to for an absorbed CO to undergo dissociation it must be bonded side-on to the metal, not end-on.

(ii) Propagation:

$$
\begin{array}{ccccccc}
CH_3 & CH_3 & & CH_3CH_2 & & RCH_2CH_2 \\
| & | & & | & & | \\
M & + & M & \longrightarrow M & + & M & \longrightarrow \longrightarrow M
\end{array}
$$

(iii) Termination:

$$
\begin{array}{cccccc}
RCH_2CH_2 & H & & & H \\
| & | & & & | \\
M & + & M & \longrightarrow RCH_2CH_3 & + & M
\end{array}
$$

$$
\begin{array}{cccc}
M & & & H \\
| & & & | \\
RCH_2CH_2 & \longrightarrow R-CH=CH_2 & + & M
\end{array}
$$
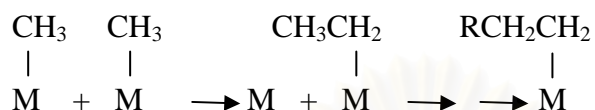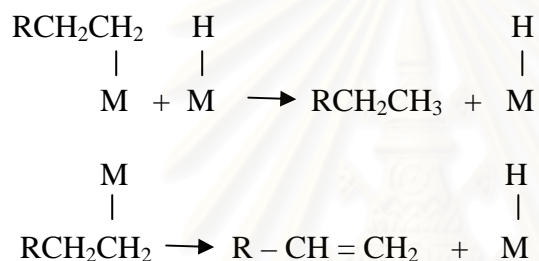
The carbide mechanism has survived the several decades since its introduction. Several items of evidence arising from recent investigation support this mechanism e.g.

(a) In the hydrogenation of CO over clean Ni surface it has been observed that CO_2 evolution proceeds that CH_4 thus

$$2CO \longrightarrow C(ad) + CO_2$$

$$C(ad) + 2H_2 \longrightarrow CH_4$$
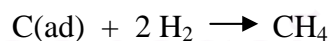
(b) Decompositon of diazomethane(CH_2N_2) at 200°c in the presence of H_2 over Co, Fe and Ru catalysts gives linear alkanes and olefins with distribution similar to that obtained from CO/H_2 reaction over the same cayalyst.

(c) Distribution of ^{13}C in $CH_2=CH$ formed when ^{13}CO, H_2- and $^{12}CH_2N_2$

were reacted under Fischer-Tropsch conditions is consistent with the distribution predicted based on the carbided mechanism and inconsistent with other proposed mechanism.

However, a drawback of this mechanism is that it does not explain the formation of oxygenated products.

3.6.2 The hydroxycarbene mechanism

(i) Initiation:

(ii) Propergation:

(iii)Termination:

RCH₂   OH

    \\   /

     C $\xrightarrow{\text{MH}}$ $RCH_2CH_3 + H_2O$

     ‖ $\xrightarrow{\text{MH}}$ $+ H_2O$

     M $\xrightarrow{\text{MH}}$ RCH_2CH_2OH

   /////
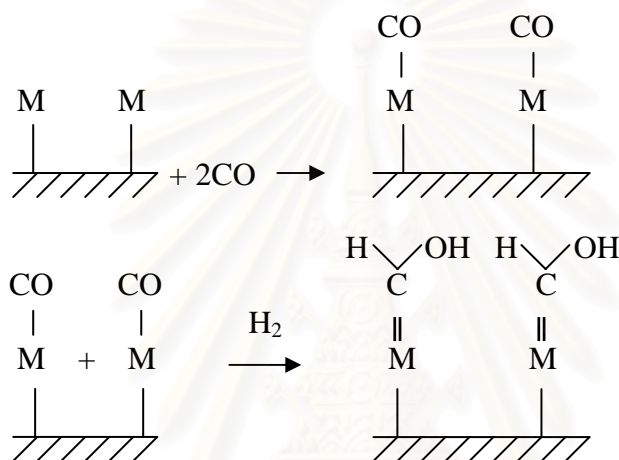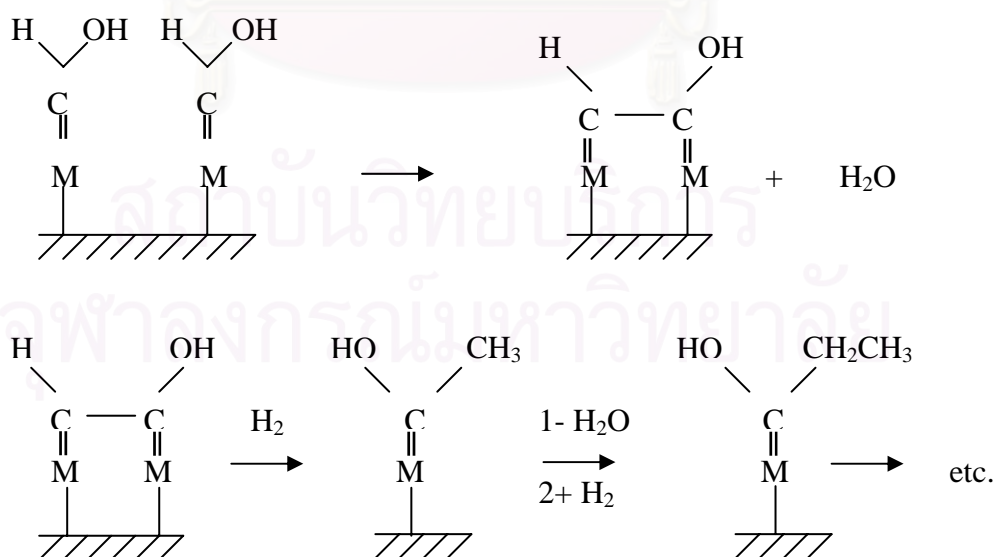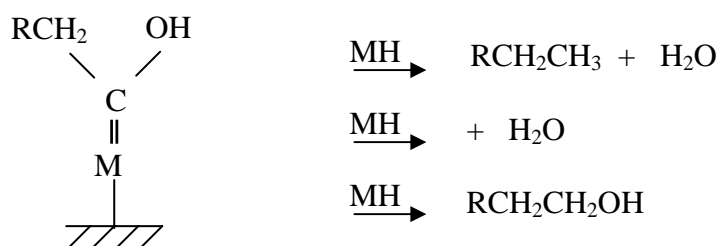
This mechanism explains the formation of alkanes, and olefins as well as oxygenated hydrocarbons. However, it precludes the dissociation of CO, which is not consistent with many experimental observations.

3.6.3 The CO insertion mechanism.

(i) initiation :

The initiation of active species is similar to that of the carbide mechanism although the mechanism of its formation is different.

O

C   H   H   CO

| | \\   /

M + M $\longrightarrow$ M

               H   CH₂OH

               | |

H-M-C=O + M $\longrightarrow$ M

CH₂OH   H   CH₃

| | |

M   +   M $\longrightarrow$ M + H₂O
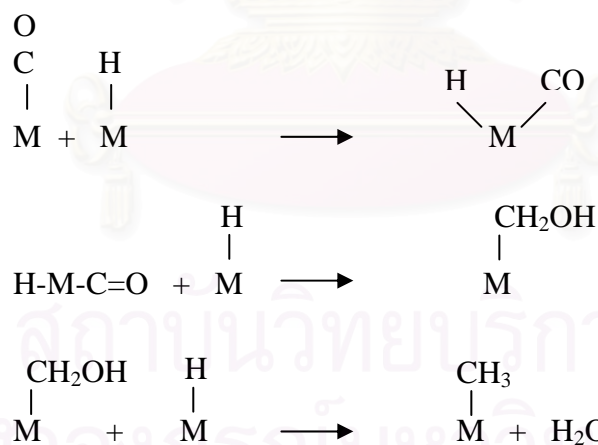
(ii) Propagation:

propagation proceeds via CO insertion rather than $-CH_2-$ insertion.

$$CH_3-M \;+\; CO \;\longrightarrow\; \underset{M}{\overset{CH_3-C=O}{|}}$$

$$\underset{M}{\overset{CH_3-C=O}{|}} \;\xrightarrow[(H_2)]{MH}\; \underset{M}{\overset{CH_3-CHOH}{|}} \;\xrightarrow[-H_2O]{MH}\; \underset{M}{\overset{CH_3-CH_2}{|}} \;\xrightarrow[(2)H_2]{MH}\; etc.$$

(iii) Termination:

$$\underset{M}{\overset{RCH_2CH_2}{|}} \;\xrightarrow{MH}\; RCH_2CH_3$$

$$\longrightarrow\; RCH=CH_2 \;+\; \underset{M}{\overset{H}{|}}$$

$$\underset{M}{\overset{R-CHOH}{|}} \;\xrightarrow{MH}\; RCH_2OH$$
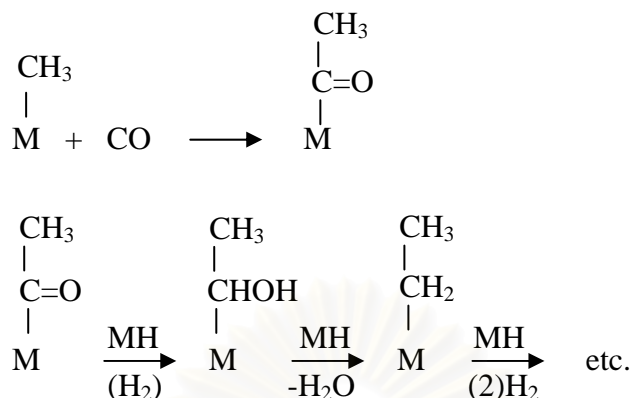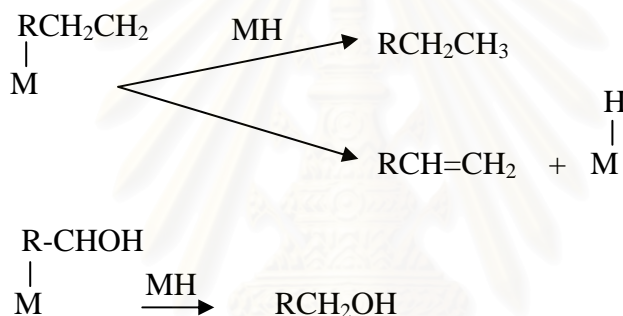
Normally, catalysts used for FTS are group VIII metals. By nature, the hydrogenation activity increases in order of Fe < Co < Ni < Ru. Ru is the most active. Ni forms predominantly methane, while Co yields much higher ratios of paraffins to olefins and much less oxygenated products such as alcohols and aldehydes than Fe does.

The current main goal in FTS is to obtain high molecular weight, straight chain hydrocarbons. However, methane and other light hydrocarbons are always present as less desirable products from the synthesis. According to the Anderson-Schulz-Flory (ASF) product distribution, typically 10 to 20% of products from the synthesis are usually light hydrocarbon (C_1-C_4). These light alkanes have low boiling points and exist in the gas phase at room temperature, which is inconvenient for transportation. Many attempts have been made to minimize these by-products and increase the yield of long chain liquid hydrocarbons by improving chain growth

probability. It would be more efficient to be able to convert these less desirable products into more useful forms, rather than re-reforming them into syngas and recycling them (Farrauto and Bartholomew, 1997). Depending upon the type of catalyst used, promoters, reaction conditions (pressure, temperature and H_2/CO ratios), and type of reactors, the distribution of the molecular weight of the hydrocarbon products can be noticeably varied.

Fischer-Tropsch synthesis (FTS) that discovered by Fischer and Tropsch over 77 years ago, as an alternate process, can convert the synthesis gas (H_2/CO) derived from carbon sources such as coal, peat, biomass and natural gas, into hydrocarbons and oxygenates. During the past decades, FTS has been developed continuously by many researchers, although the rise and fall in research intensity on this process has been highly related to the demands for liquid fuels and relative economics. This synthesis is basically the reductive polymerization (oligomerization) of carbon monoxide by hydrogen to form organic products containing mainly hydrocarbons and some oxygenated products in lesser amounts. The main reactions of FTS are:

$$CO + \left(1 + \frac{m}{2n}\right)H_2 \rightarrow \left(\frac{1}{n}\right)C_nH_m + H_2O \qquad (3.1)$$

$$CO + 3H_2 \rightarrow CH_4 + H_2O \qquad (3.2)$$

$$CO + H_2O \rightarrow CO_2 + H_2 \qquad (3.3)$$

$$2CO \rightarrow C + CO_2 \qquad (3.4)$$
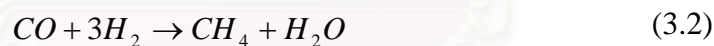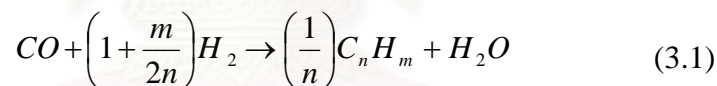
Equation (3.1) is the formation of hydrocarbons higher than C1, and the equation (3.2) is methanation. The water-gas shift reaction, which is undesirable for natural gas conversion, is shown in equation (3.3). The Boudouard reaction, which results in carbon deposition on the catalyst surface, is shown in equation (3.4).

The mechanism consists of surface steps in five categories: (1) the adsorption of reactants (H_2 and CO); (2) chain initiation; (3) chain propagation; (4) chain termination and desorption of products; (5) readsorption and secondary reaction of olefins. Depending upon the type of catalyst used, promoters, reaction conditions (pressure, temperature and H_2/CO ratios), and type of reactors, the distribution of the molecular weight of the hydrocarbon products can be noticeably varied.

Normally, catalysts used for this synthesis are group VIII metals. By nature, the hydrogenation activity increases in order of Fe < Co < Ni < Ru. Ru is the most active. Ni forms predominantly methane, while Co yields much higher ratios of paraffins to olefins and much less oxygenated products such as alcohols and aldehydes than Fe does.

With regards to the operating conditions, usually higher pressures will result in higher rates. Entrained bed reactors or slurry bubble column reactors are better than fixed-bed reactors for FTS since they can remove heat from this exothermic synthesis, allowing better temperature control.

The current main goal in using FTS is to obtain high molecular weight, straight chain hydrocarbons. However, methane and other light hydrocarbons are always present as less desirable products from the synthesis. According to the Anderson-Schulz-Flory (ASF) product distribution, typically 10 to 20% of products from the synthesis are usually light hydrocarbon (C_1-C_4) these light alkanes have low boiling points and exist in the gas phase at room temperature, which is inconvenient for transportation. Many attempts have been made to minimize these byproducts and increase the yield of long chain liquid hydrocarbons by improving chain growth probability. It would be more efficient to be able to convert these less desirable products into more useful forms, rather than re-reforming them into syngas and recycling them.

CHAPTER IV

EXPERIMENTAL

This chapter consists of experimental systems and procedures used in this work which is divided into third parts including sample preparation, characterization and reaction study in CO hydrogenation.

The first part (section 4.1) is described chemical of each sample, synthesis of TiO_2 nanocrystal in anatase phase via sol-gel process and Preparation of Co/TiO_2 catalyst. The second section (section 4.2) is explained characterization by various techniques including of XRD, temperature-programed reduction (TPR), H_2 Chemisorption, SEM, TEM, N_2 physisorption. Finally, the last part (section 4.3) is illustrated catalyst activity measurement in CO hydrogenation.

4.1 Sample preparations

4.1.1 Chemicals

The lists of chemicals used in this research are shown in the Table 4.1.

Table 4.1: Chemicals used for sample preparations

Chemical	Grade	Supplier
Titanium isopropoxide	99.999%	Aldrich
Cobalt (II) nitrate hexahydrate	analytical	Aldrich
Ethanol	andydrous	Aldrich

4.1.2 Synthesis of TiO$_2$ nanocrystal in anatase phase having different amounts of bulk and surface defects via sol-gel

TiO$_2$ nanocrystals were synthesized via sol-gel process of titanium ethoxide. A specific amount of precursor was dissolved in ethanol, and mixed with a water-ethanol solution at water:alkoxide molar ratio equal to 165. A precursor solution was added drop-wise into the aqueous solution and was stirred by ultrasonic vibration at room temperature. White precipitates of hydrous oxides formed instantly and the mixture was stirred for at least 2h. The amorphous precipitates were separated from the mother liquor by centrifugation and were redispersed in ethanol for five times to minimize particle agglomeration. The resulting materials were then dried and calcined at 450 ^{o}C in the studied atmospheres, respectively, for 2 h with the heating rate at 10 ^{o}C/min. To study the controlling of surface defect in the first step, the water:alkoxide molar ratio used during sol-gel synthesis which is the studied parameter was also varied from 4 to 165. Details of calculation for evaluating water:alkoxide molar ratio in this synthesis are given in Appendix A.

4.1.3 Preparation of Co/TiO$_2$ catalyst

A 20 wt% of Co/TiO$_2$ was prepared by the incipient wetness impregnation [25]. A designed amount of cobalt nitrate [Co(NO$_3$)·6H$_2$O] was dissolved in deionized water and then impregnated onto TiO$_2$ supports obtained from 2.1. The catalyst precursor was dried at 110 ^{o}C for 12 h and calcined in air at 450 ^{o}C for 4 h. Details of calculation of this preparation are given in Appendix A.

4.2 Characterization

4.2.1 Powder X-ray diffraction (XRD)

X-ray diffraction (XRD) was performed by using a SIEMENS XRD D5000 connected with a computer using Diffract ZT version 3.3 program for fully control of the XRD analyzer. The measurements were carried out using Ni-filtered CuK$_\alpha$ (λ=1.54439Å) radiation. Scans were performed over the range from 10° to 80° with step 0.02^o. To determine the average crystallite size, peak-broadening analysis was applied to anatase (101) peak using Scherrer's equation.

4.2.2 Temperature-programmed reduction

TPR was used to determine the reduction behaviors of the samples. It was carried out using 20 mg of a sample and a temperature ramp from 35 to 800^oC at 10^oC/min. The carrier gas was 5% H_2 in Ar. A cold trap was placed before the detector to remove water produced during the reaction. A thermal conductivity detector (TCD) was used to determine the amount of H_2 consumed during TPR. The H_2 consumption was calibrated using TPR of Ag_2O at the same conditions . Details of calculation for reducibility of the sample are given in Appendix B.

4.3.3 Hydrogen chemisorption

Static H_2 chemisorption at 100^oC on the reduced sample was used to determine the number of reduce surface cobalt metal atoms and overall cobalt dispersion. H_2 chemisorption was carried out following the procedure described by Reuel and Bartholomew [26] using a Micromeritics Pulse Chemisorb 2700 instrument. Prior to chemisorption, the samples were reduced at 350^oC for 10 h. Details of calculation for reducibility of the sample are given in Appendix C.

4.2.4 Scanning electron microscopy

SEM was used to determine morphology of the secondary particle of catalyst. The SEM of JEOL mode JSM-5410LV was applied using the secondary electron mode at 15 kV.

4.2.5 Transmission electron microscopy

The morphology and size of the secondary particle of catalysts were determined using a JEOL-TEM 200CX transmission electron spectroscopy operated at 100 kV.

4.2.6 N_2 physisorption

Surface area (BET) of the sample was measured by N_2 physisorption using a micromeritics model ASAP 2000 using nitrogen as the adsorbate. Each sample was degassed under vacuum at < 10 μm-Hg in the Micromeritics ASAP 2000 at 150 ^{o}C for 4 h prior to N_2 physisorption.

4.3 Reaction study in CO hydrogenation

4.3.1 Materials

The reactant gas used for the reaction study was the carbon monoxide in hydrogen feed stream as supplied by Thai Industrial Gas Limited (TIG). The gas mixture contained 9.73 vol % CO in H_2 (22 CC/min). The total flow rate was 30 CC/min with the H_2/CO ratio of 10/1. Ultra high purity hydrogen (50 CC/min) and high purity argon (8 CC/min) manufactured by Thai Industrial Gas Limited (TIG) were used for reduction and balanced flow rate

4.3.2 Apparatus

Flow diagram of CO hydrogenation system is shown in Figure 4.1. The system consists of a reactor, an automatic temperature controller, an electrical furnace and a gas controlling system.

4.3.2.1 Reactor
The reactor was made from a stainless steel tube (O.D. 3/8"). Two sampling points were provided above and below the catalyst bed. Catalyst was placed between two quartz wool layers.

4.3.2.2 Automation Temperature Controller
This unit consisted of a magnetic switch connected to a variable voltage transformer and a solid-state relay temperature controller model no. SS2425DZ connected to a thermocouple. Reactor temperature was measured at the bottom of the catalyst bed in the reactor. The temperature control set point is adjustable within the range of 0-800°C at the maximum voltage output of 220 volt.

4.3.2.3 Electrical Furnace
The furnace supplied heat to the reactor for CO hydrogenation. The reactor could be operated from temperature up to 800°C at the maximum voltage of 220 volt.

4.3.2.4 Gas Controlling System

Reactant for the system was each equipped with a pressure regulator and an on-off valve and the gas flow rates were adjusted by using metering valves.

4.3.2.5 Gas Chromatography

The composition of hydrocarbons in the product stream was analyzed by a Shimadzu GC14B (VZ10) gas chromatograph equipped with a flame ionization detector. A Shimadzu GC8A (molecular sieve 5A) gas chromatography equipped with a thermal conductivity detector was used to analyze CO and H_2 in the feed and product streams. The operating conditions for each instrument are shown in the Table 4.2.

Table 4.2 Operating condition for gas chromatograph

Gas Chromagraph	SHIMADZU GC-8A	SHIMADZU GC-14B
Detector	TCD	FID
Column	Molecular sieve 5A	VZ10
- Column material	SUS	-
- Length	2 m	-
- Outer diameter	4 mm	-
- Inner diameter	3 mm	-
- Mesh range	60/80	60/80
- Maximum temperature	350 ^{o}C	80 ^{o}C
Carrier gas	He (99.999%)	H_2 (99.999%)
Carrier gas flow	20 cc/min	-
Column gas	He (99.999%)	Air, H_2
Column gas flow	20 cc/min	-
Column temperature		
- initial (^{o}C)	60	70
- final (^{o}C)	60	70
Injector temperature (^{o}C)	100	100
Detector temperature (^{o}C)	100	150
Current (mA)	80	-
Analysed gas	Ar, CO, H_2	Hydrocarbon C_1-C_4

4.3.3 Procedures

1. Using 0.2 g of catalyst packed in the middle of the stainless steel microrector, which is located in the electrical furnace.

2. A flow rate of Ar = 8 cc/min, 9% CO in H_2 = 22 cc/min and H_2 = 50 cc/min in a fixed-bed flow reactor. A relatively high H_2/CO ratio was used to minimize deactivation due to carbon deposition during reaction.

3. The catalyst sample was re-reduce *in situ* in flowing H_2 at 350 ^{o}C for 3 h prior to CO hydrogenction.

4. CO hydrogenation was carried out at 220 ^{o}C and 1 atm total pressure in flowing 9% CO in H_2.

5. The effluent was analyzed using gas chromatography technique. [Thermal Conductivity Detector (TCD) was used for separation of carbon monoxide (CO) and methane (CH_4) and flame ionization detector (FID) were used for separation of light hydrocarbon such as methane (CH_4), ethane (C_2H_6), propane (C_3H_8), etc.] In all cases, steady-state was reached within 6 h.

Details of calibration curves of composition of reactant and products in CO hydrogenation are given in Appendix D

Details of calculation for %conversion and Reaction rate of the sample are given in Appendix E.
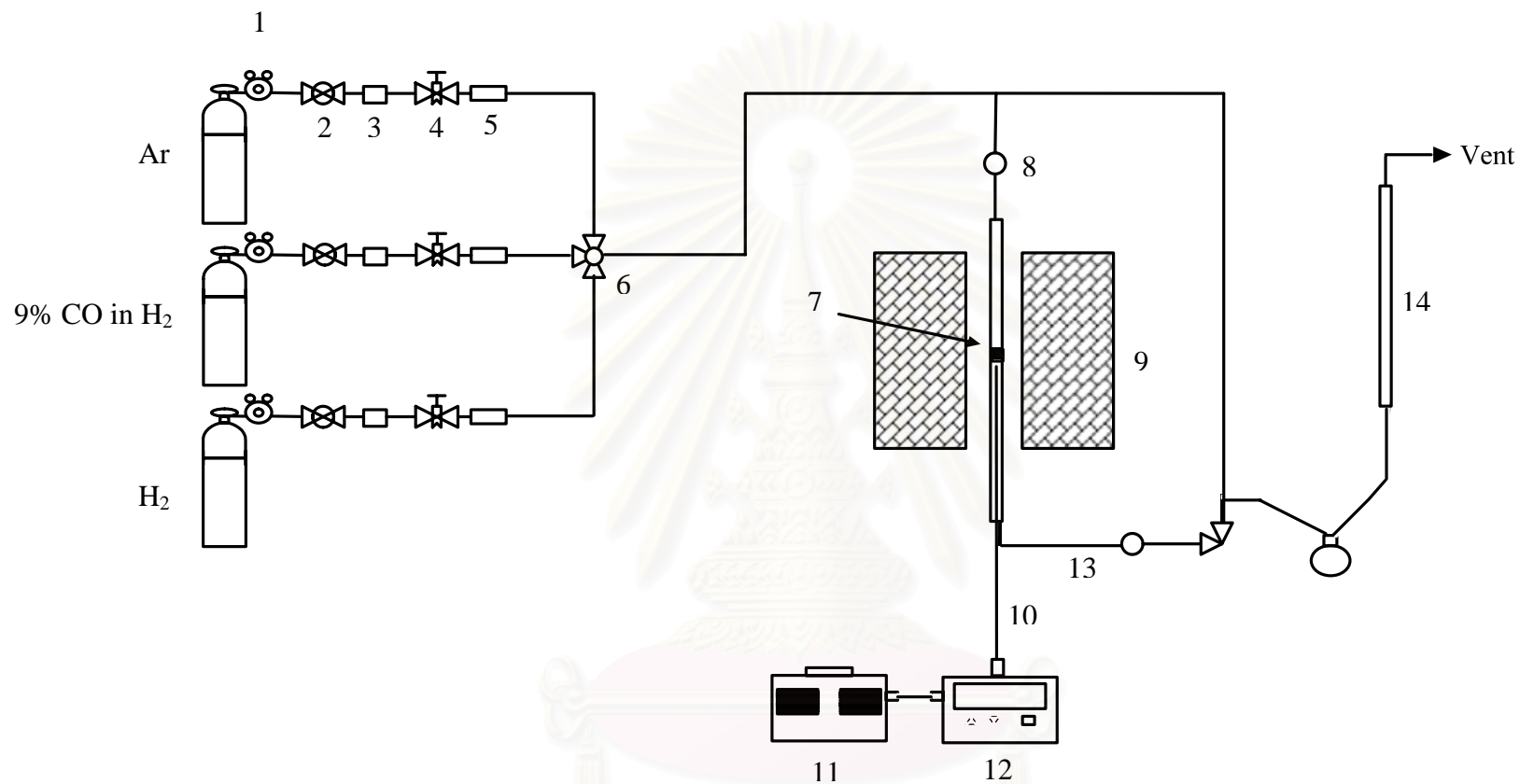
1. Pressure Regulator   2. On-Off Value   3. Gas Filter   4. Metering Valve
5. Back Pressure   6. 3-way Valve   7.Catalyst Bed   8. Sampling point
9. Furnace   10. Thermocouple   11. Variable Voltage Transformer   12. Temperature Controller
13. Heating Line   14. Bubble Flow Meter

Figure 4.1 Flow diagram of CO hydrogenation system

RESERCH METHODOLOGY

```
┌─────────────────────────────┐
│      Literature reviews      │
└─────────────────────────────┘
              │
              ▼
```

TiO$_2$ support preparation
Synthesis of the surface and bulk defect titania supports by sol- gel method

- using water:alkoxide molar ratio 4-165

- untrasonic vibration at room temp, 2 h

- centrifugation and were redispersed in ethanol for five times

- dry in air

- calcine 450° C, 2 h

Support characterization using N$_2$ physisorption, XRD, ESR

Catalyst preparation
Preparation of Co/TiO$_2$ catalyst

-20 wt% of Co load on TiO$_2$ by impregnation

- dried at 110° C, 2 h

- calcine 500° C, 4 h

Catalyst characterization using N$_2$ physisorption, XRD, SEM, TEM, TPR, and H$_2$ chemisorption

Reaction study in CO hydrogenation at 220°C and 1 atm

Data analysis

CHAPTER V
RESULTS AND DISCUSSION

This thesis investigated effects of bulk and surface defects of TiO_2 support on the physico-chemical properties of Co/TiO_2 catalyst via methanation. In this chapter, the experimental results and discussions are described. The results and discussions are divided into four sections. First section described characteristics of TiO_2 support. Second section described characteristic of Co/TiO_2 catalyst. Third section described reduction behavior of Co/TiO_2 catalyst and the last second determined catalytic activity for CO-hydrogenation over Co/TiO_2 catalyst.

5.1 Characteristics of TiO_2 support

TiO_2 supports having different amounts of bulk and surface defects were prepared using sol-gel technique. In Figure 5.1, it showed XRD peaks of TiO_2 supports at 26°, 37°, 48°, 55°, 56°, 62°, 69°, 71° and 75°, assigned to the anatase phase TiO_2 [27]. The amounts of bulk and surface defects were monitored by the intensity of ESR spectra as shown in Figure 5.2. The ESR spectra at g = 1.974 and g = 2.003 are assigned to a surface defect (Ti^{3+}) occurring on TiO_2 support [28,29,30,31] and bulk defect present in TiO_2 support [28,32], respectively. In Table 5.1, it reveals different characteristics of TiO_2 supports named as the TiO_2-x, where x = A, B, C, D, and E indicating increased amounts of surface defect from A to E whereas the bulk defects decreased from A to E. The crystallinity of TiO_2 supports on terms of XRD peak intensity at 26° was also monitored in order to confirm the amount of bulk defect in the support. The amount of bulk defect is disproportional to the XRD peak intensity. The crystallite size and surface area are also shown in this table.

Table 5.1 Characteristics of TiO$_2$ samples

Sample	Water: Alkoxide Ratio	Crystallite Size[a] (nm)	Surface Area (m^2/g)	ESR Intensity		XRD Intensity[d]
				Ti^{3+} [b]	Bulk defect[c]	
TiO$_2$-A	165	6.9	101	300	1560	1253
TiO$_2$-B	80	7.0	99	1000	1432	1495
TiO$_2$-C	40	8.5	97	1459	1078	1652
TiO$_2$-D	16	8.9	97	1512	684	1853
TiO$_2$-E	4	9.1	96	2756	184	2278

[a] Estimated from XRD at anatase (101) peak

[b] Determined from ESR intensity at g = 1.974

[c] Determined from ESR intensity at g = 2.033

[d] Determined from XRD intensity at 2Θ = 26
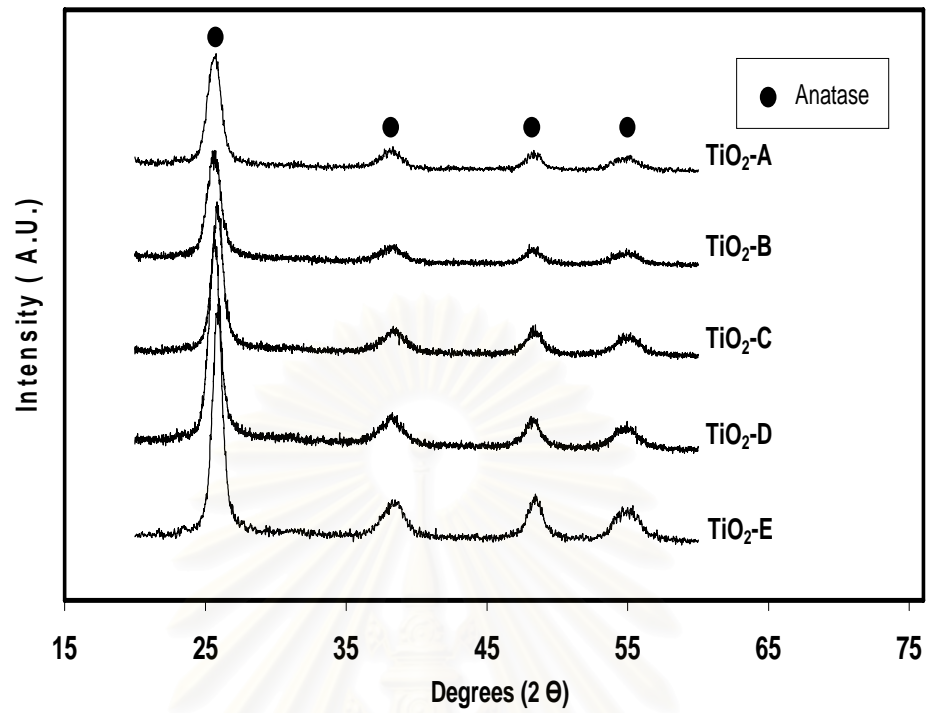
Figure 5.1 XRD patterns of resulting TiO$_2$ support by sol-gel method
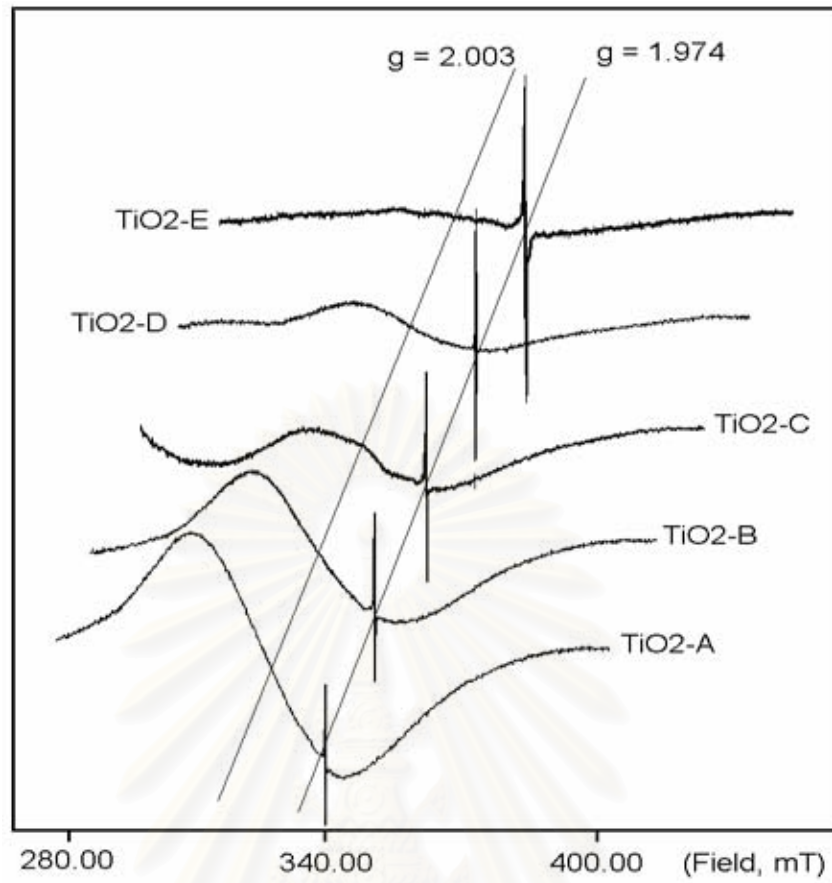
Figure 5.2 ESR spectra of resulting TiO$_2$ support by sol-gel method

5.2 Characteristic of Co/TiO$_2$ catalyst

A 20% wt of cobalt was impregnated onto different TiO$_2$ supports having various amounts of bulk and surface defects. After calcination in air at 500 ^{o}C for 5 h, all Co/TiO$_2$ catalysts were tested by XRD as shown in Figure 5.3. It showed that all Co/TiO$_2$ catalysts exhibited mainly two XRD patterns including (i) the patterns for TiO$_2$ support in anatase phase (26°, 37°, 48°, 55°, 56°, 62°, 69°, 71° and 75°) and (ii) the patterns for Co$_3$O$_4$ formed after calcination (36°, 46° and 65°) [3]. The surface areas after calcination of Co/TiO$_2$-x where x = A, B, C, D, E D, E were at 30, 21, 13, 24 and 55 m^2/g.cat , respectively.
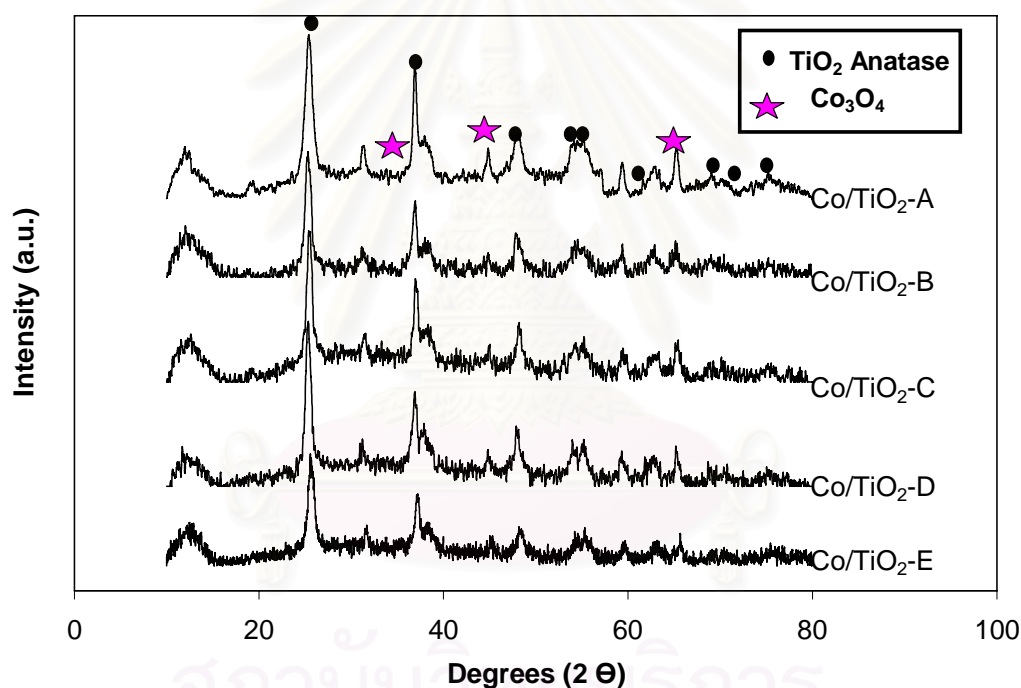

Figure 5.3 XRD patterns of Co/TiO$_2$ catalyst

For crystallinity of TiO$_2$ support, it showed that all impregnated TiO$_2$ supports have the same level of crystallinity referring the same level of bulk defect after calcination at 500°C for 5 hrs of Co/TiO$_2$ catalyst. This is because the crystalline TiO$_2$ structure has enough energy to rearrange its crystal structure by removing bulk defect as shown in the Scheme 5.1 corresponding with the report of Jung et al. [10]. However, during calcination, the cobalt oxide formed during rearranging the crystal

structure of TiO$_2$ support having low and high amount of bulk defect was still unclear, so that, more characterization techniques have been used to clarify the physico-chemical properties of cobalt on TiO$_2$ support.
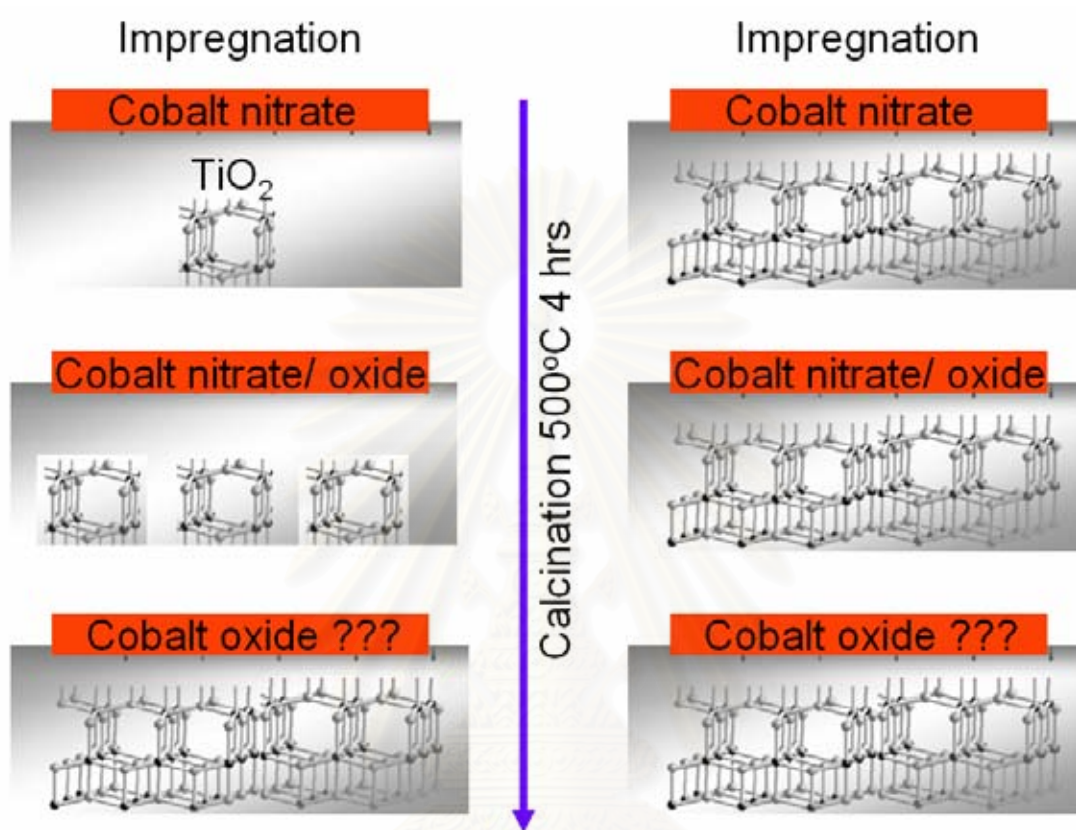
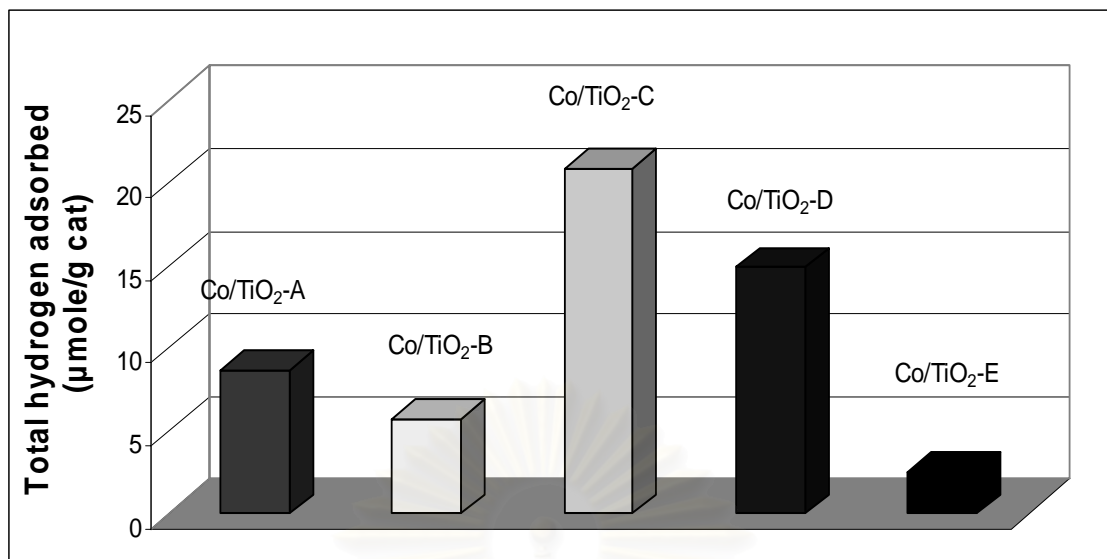**Scheme 5.1** The reduction of bulk defect during calcination of Co/TiO$_2$ catalyst

**Figure 5.4** Total hydrogen chemisorption on Co/TiO$_2$ catalyst

The total amount of H$_2$ chemisorbed on Co/TiO$_2$ catalysts was determined using H$_2$-chemisorption as shown in the Figure 5.4. It showed that amounts of H$_2$ chemisorbed on Co/TiO$_2$ catalysts reached to the maximum point for the Co/TiO$_2$-C, which was prepared by impregnated cobalt nitrate onto the TiO$_2$ support having the lower amount of bulk defect and higher amount of surface defect compared to the Co/TiO$_2$-A sample. However, after the Co/TiO$_2$ catalyst prepared by impregnated the cobalt nitrate onto TiO$_2$ support having more amount of bulk defect and less amount of surface defect, the total amount of H$_2$ chemisorbed on Co/TiO$_2$ catalyst became lower.

Based on our previous work regarding to the study of effect of surface defect of TiO$_2$ support (with the same level of bulk defect, confirmed by the results of ESR and XRD) on the characteristics and catalytic properties of Co/TiO$_2$ catalyst, it was shown that the surface defect of TiO$_2$ support during impregnating cobalt nitrate can increase the amount of total H$_2$ chemisorp on Co/TiO$_2$ catalyst [8]. This is attributed to surface defect of TiO$_2$ support can increase the interaction of cobalt nitrate and TiO$_2$ support resulting in the increase of cobalt dispersion on TiO$_2$ support after calcination at 500°C for 5 hrs as shown in the Scheme 5.2.
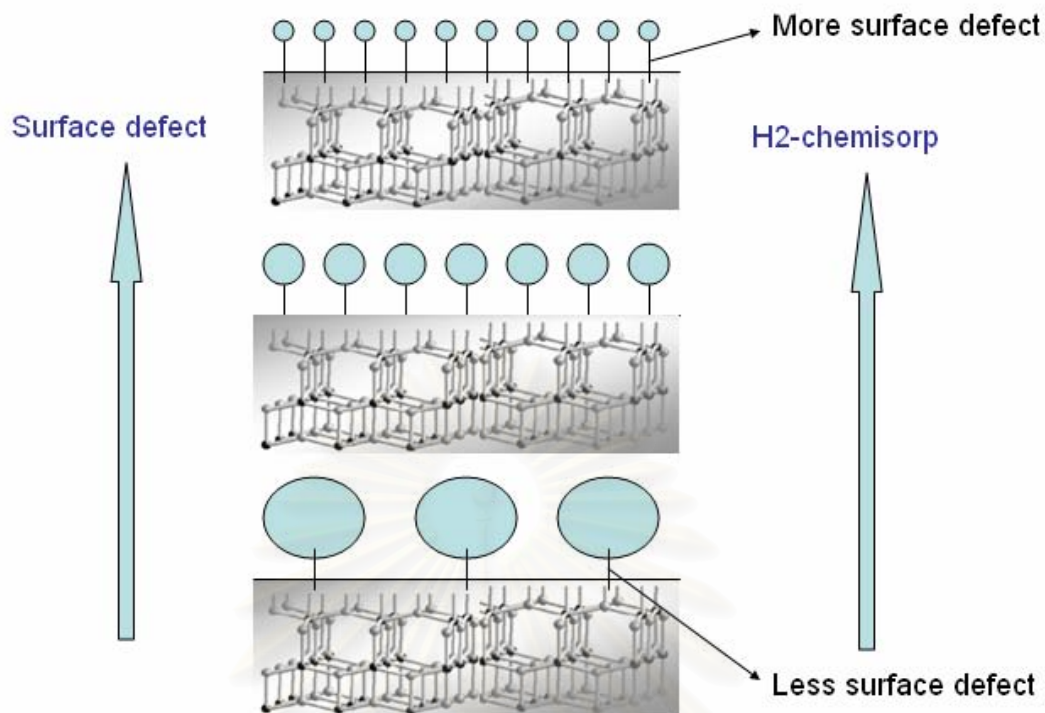
Scheme 5.2 The influence of surface defect on cobalt dispersion on TiO_2 support

However, this work demonstrated that, although, the Co/TiO_2 support has been prepared by impregnated cobalt nitrate onto TiO_2 support having higher surface defect, the total H_2 chemisorption became lower on the samples Co/TiO_2-D and Co/TiO_2-E. It inferred that the amount of bulk defect of TiO_2 support during impregnating cobalt nitrate is also another main parameter controlling the characteristics properties of Co/TiO_2 catalyst consequently controlling total H_2 chemisorption on Co/TiO_2 catalyst.
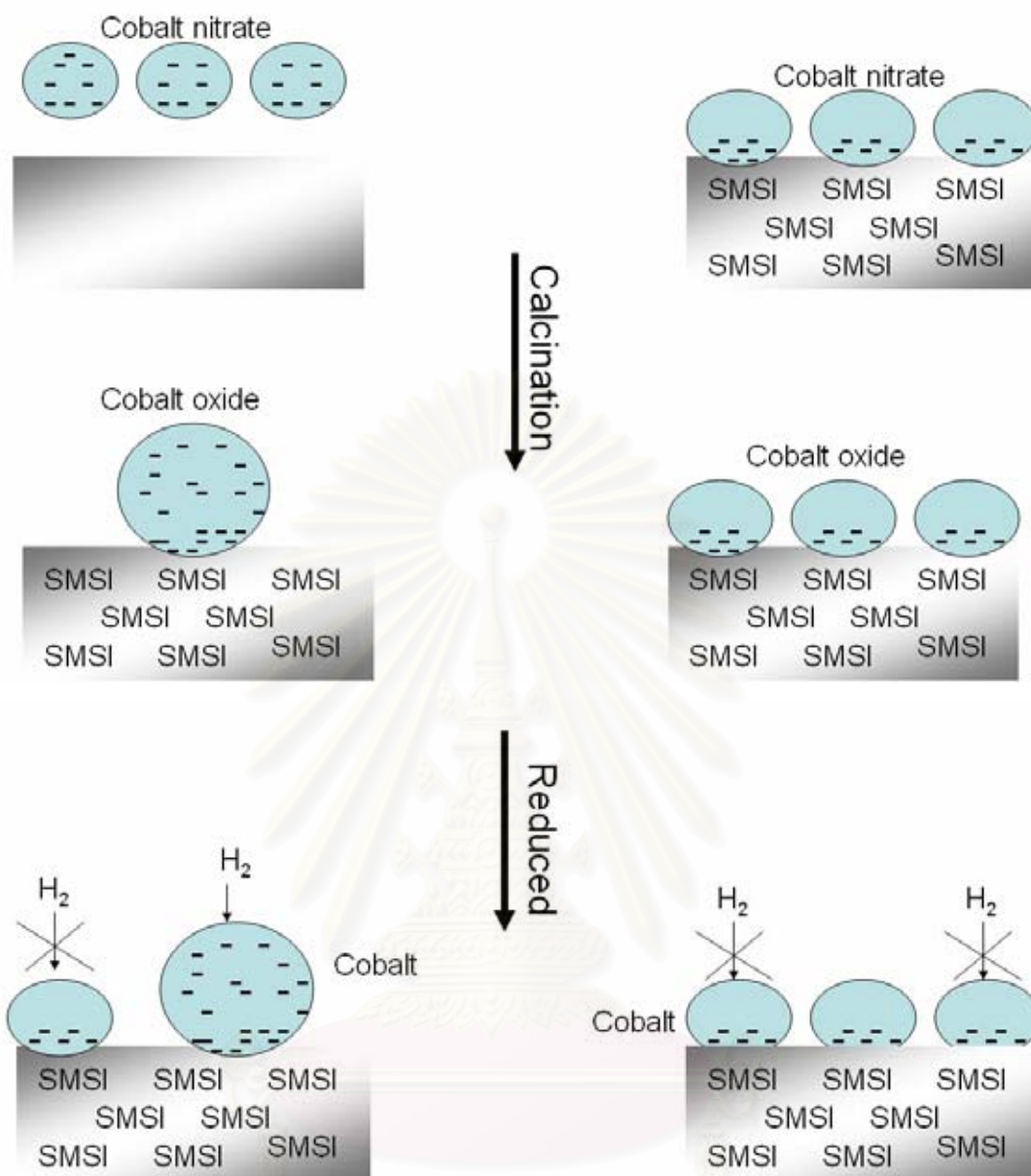
Scheme 5.3 The effect of bulk defect (SMSI) of TiO_2 support during impregnating cobalt nitrate on the amount of H_2 chemisorption on Co/TiO_2 catalyst

Goodman et al. [34] reported that a decrease of total H_2 chemisorption on TiO_2-supported catalyst is attributed to (i) a decrease of cobalt dispersion on support or/and (ii) a rich of electron at the interface of cobalt and TiO_2 support becoming low electron density at the exposure cobalt surface to H_2. However, in this work, the total H_2 chemisorption decreased when the cobalt has more dispersion on TiO_2 support (because of the increase of surface defect [34]). So that, the main reason of a decrease

of total H_2 chemisorption should be attributed to the rich of electron at cobalt-TiO$_2$ interface which occurs when cobalt was supported on high SMSI support. Based on previous work, it was shown that surface defect has no effect on SMSI property of TiO$_2$ support because there are not a decrease of total H_2 chemisorption when cobalt was supported on TiO$_2$ having more surface defect (SMSI property are (i) higher metal dispersion and (ii) low amount of H_2 chemisorption [34]). In this work, not only surface defect of TiO$_2$ support has been studied but bulk defect of TiO$_2$ support has also been studied. Therefore, we inferred that the amount of bulk defect of TiO$_2$ support during impregnating cobalt nitrate should have the effect to the amount of H_2 chemisorption on Co/TiO$_2$ catalyst or SMSI property. Based on this work, therefore, it can infer that a decrease of amount of bulk defect (higher crystallinity) can enhance the SMSI property of TiO$_2$ support. So that is why the amorphous TiO$_2$ (too much amount of bulk defect) has no SMSI property.

However, XRD showed that the crystallinity (bulk defect) became the same level after calcination TiO$_2$-supported cobalt nitrate; therefore, all Co/TiO$_2$ catalyst should has the same level of SMSI property after calcination. However, from H_2-chemisorption result, it showed that the rich of electron between cobalt-TiO$_2$ interfaces became higher (interpreted from the losses of H_2-chemisorp even the cobalt dispersion increased). This matter can be explained by the amount of bulk defect of TiO$_2$ support during impregnating cobalt nitrate as seen in Scheme 5.3.

As discussed above that the TiO$_2$ support having lower bulk defect (or crystallinity) should has more SMSI property (so that the amorphous TiO$_2$ do not have this property). Scheme 5.3 showed that bigger particle size of cobalt oxide would be form after calcination cobalt nitrate which was supported on TiO$_2$ having low SMSI property (high amount of bulk defect). Although, the SMSI property of all TiO$_2$ support would be the same after calcination process, the final particle size of all cobalt oxides are still different based on the SMSI property of TiO$_2$ support during the impregnation method. This is because there are higher migration rate of cobalt nitrate/ oxide on the TiO$_2$ having lower SMSI property than another one. Although, the final TiO$_2$ support after calcination has the same SMSI property, in case of bigger cobalt particle site (occur from the supporting cobalt nitrate onto TiO$_2$ support having higher bulk defect or lower SMSI property), the SMSI of support might not have enough

potential to attract all electron in cobalt particle to the cobalt-TiO$_2$ interface. Therefore, the overview of electron density is still dispersed throughout the cobalt particle. For another case, when the cobalt nitrate was support onto the TiO$_2$ support having higher SMSI property, the migration rate of cobalt nitrate/oxide would be small, so that, the particle size of cobalt would be also small. Therefore, the SMSI of support should have enough potential to attract all electrons in cobalt particle to the cobalt-TiO$_2$ interface resulting in un-chemisorption of H$_2$ on cobalt. Therefore, it can concluded that the decrease of total H$_2$-chemisorption on the sample Co/TiO$_2$-D and Co/TiO$_2$-E is attributed to cobalt nitrate was impregnated onto TiO$_2$ support having high SMSI property (less amount of bulk defect) resulting in the rich electron at the cobalt-TiO$_2$ interface and finally the H$_2$ can not chemisorb on its cobalt surface. Therefore, this work can prove that besides the surface defect on TiO$_2$ support during impregnation method, the bulk defect of TiO$_2$ support during impregnation method can also control the characteristics of Co/TiO$_2$ catalyst and the amount of surface and bulk defect used during impregnating cobalt nitrate should be optimal.

SEM was conducted in order to study the morphologies of the samples as shown in the Figure 5.5 a-e. The agglomeration of secondary particles of Co/TiO$_2$ catalyst was observed throughout the catalyst granules for all catalysts. In general, there was no significant change in morphologies after calcination except for the Co/TiO$_2$-E catalyst. The bigger size of secondary particle for Co/TiO$_2$-E was evident (0.5 microns). In order to determine the dispersion of cobalt oxide species on the various TiO$_2$ supports, the more powerful technique such as TEM was applied to all the samples as shown in the Figure 5.6 a-e. However, considering the morphologies for the cobalt oxide species (Co$_3$O$_4$) dispersed on the support, they could not be differentiated between those and the supports. It was suggested that the morphologies of cobalt oxide species were essentially similar for all TiO$_2$ supports. In case of the primary particle size, it showed that the Co/TiO$_2$-E exhibited the biggest primary particle size among other samples. This should be related to the biggest secondary particle as seen for SEM.
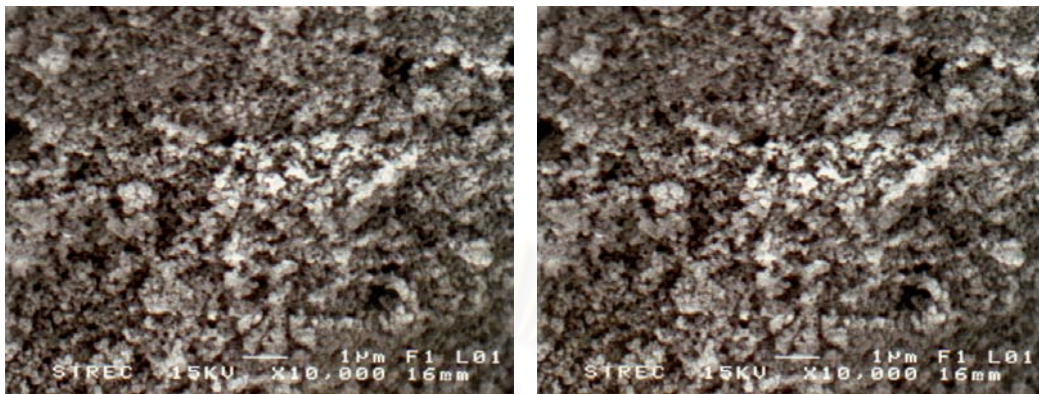
(a) Co/TiO$_2$-A

(b) Co/TiO$_2$-B
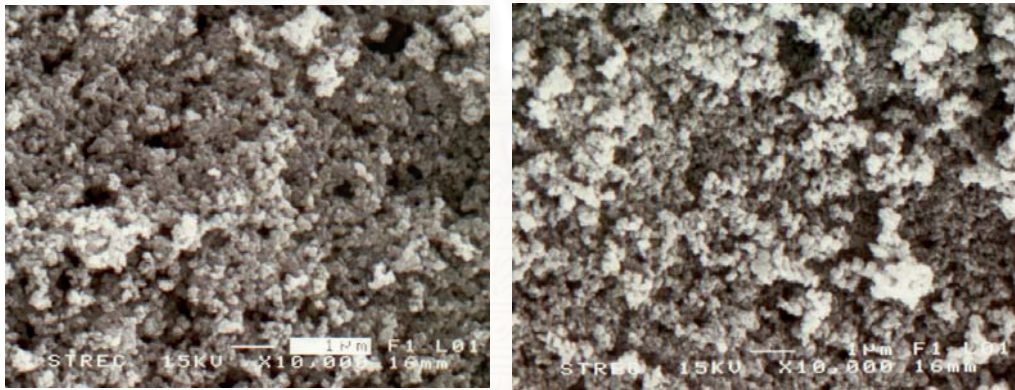
(c) Co/TiO$_2$-C

(d) Co/TiO$_2$-D

(e) Co/TiO$_2$-E

Figure 5.5 SEM micrograph of Co/TiO$_2$ catalyst
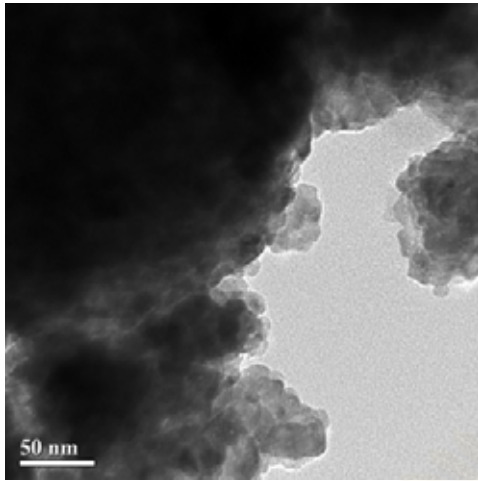
(a) Co/TiO$_2$-A
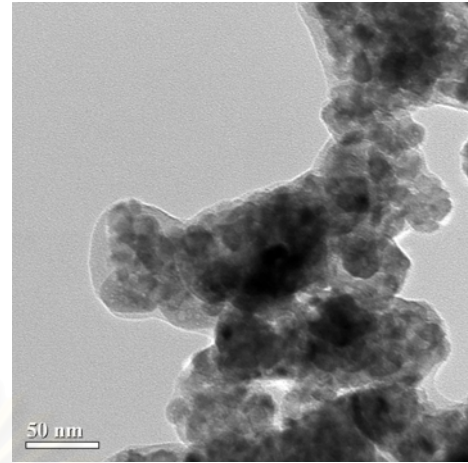
(b) Co/TiO$_2$-B
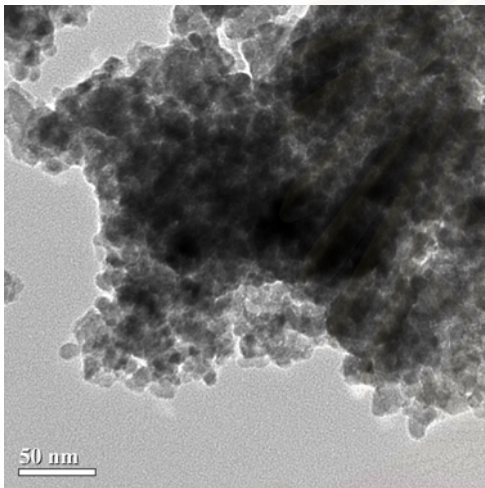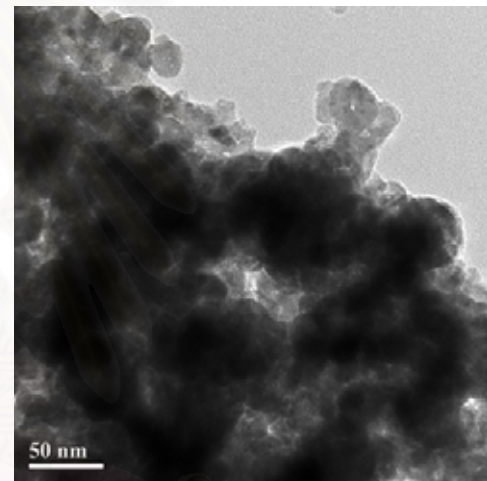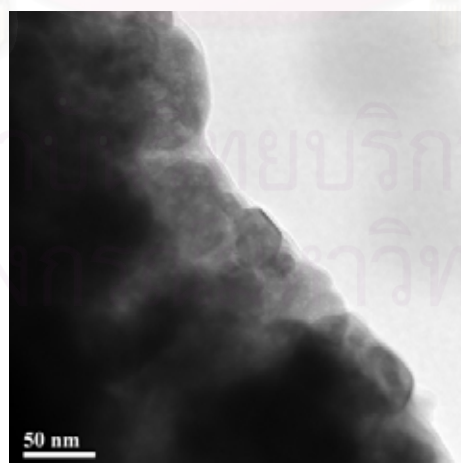
(c) Co/TiO$_2$-C

(d) Co/TiO$_2$-D

(e) Co/TiO$_2$-E

Figure 5.6 TEM micrograph of Co/TiO$_2$ catalyst

5.3 Reduction behavior of Co/TiO$_2$ catalyst

The TPR profiles of various Co/TiO$_2$ catalysts are shown in the Figure 5.7. All Co/TiO$_2$ catalysts exhibited three reduction peaks representing the reduction of Co$_3$O$_4$ to Co^o. The reducibility of Co/TiO$_2$ catalyst was also estimated from the peak area of TPR as shown in Figure 5.8. It showed that reducibility reached to a maximum point for the Co/TiO$_2$-B, which was prepared by impregnated cobalt nitrate onto the TiO$_2$ support having the lower amount of bulk defect and higher amount of surface defect compared to the Co/TiO$_2$-A sample. However, after the Co/TiO$_2$ catalyst prepared by impregnated the cobalt nitrate onto TiO$_2$ support having more amount of bulk defect and less amount of surface defect, the reducibility of Co/TiO$_2$ catalyst became lower.
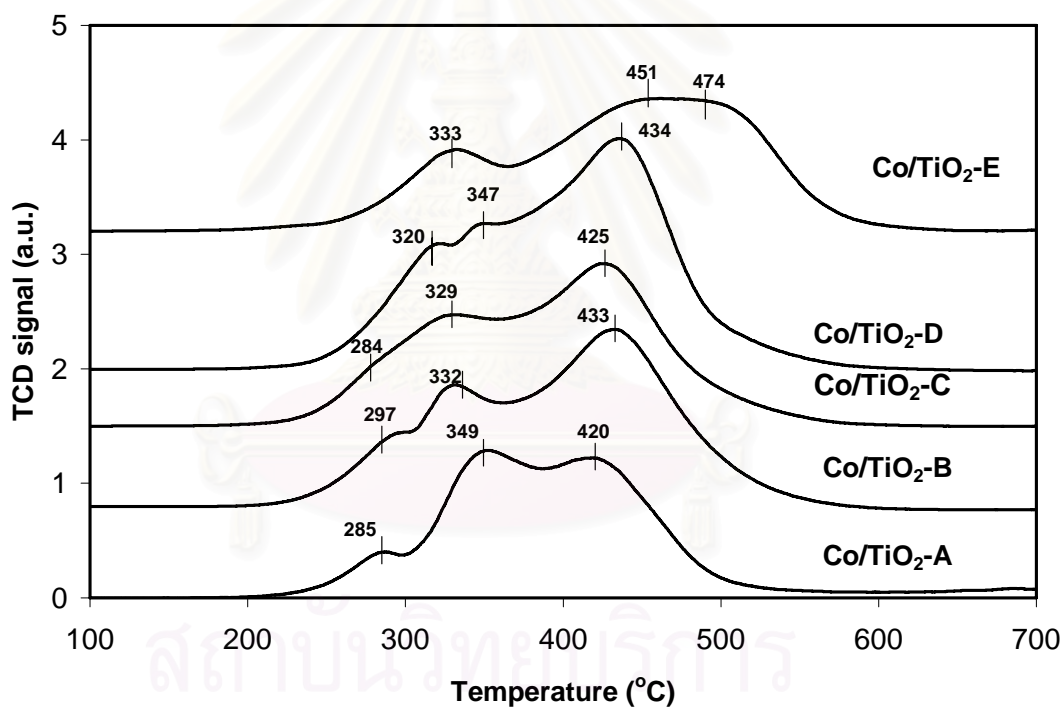
Figure 5.7 TPR profile of Co/TiO$_2$ catalyst
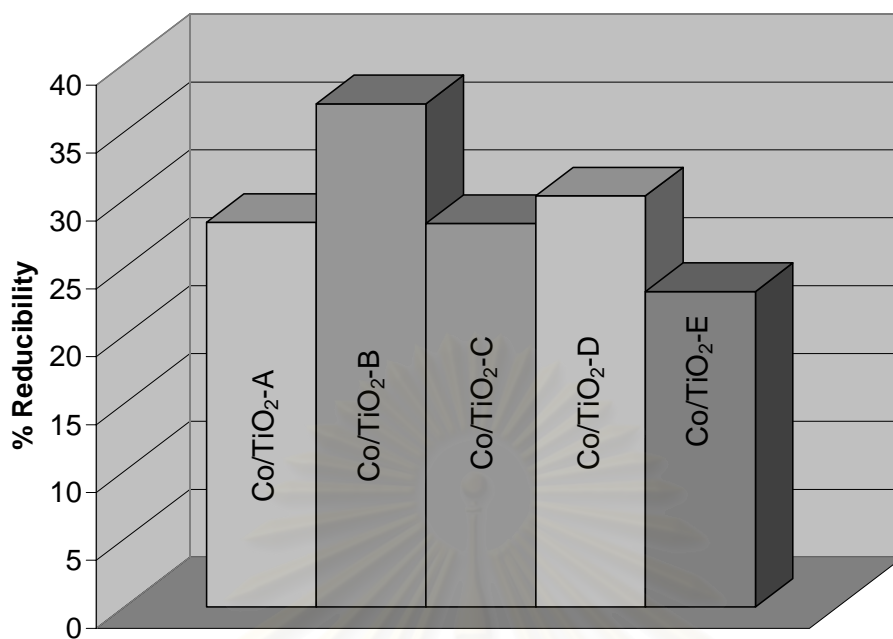
Figure 5.8 Reducibility of Co/TiO_2 catalyst

The reduction temperatures of each reduction peaks are also illustrated in the Figure 5.9 a-c. It showed that the reduction temperature of all reduction peaks became higher when the Co/TiO_2 catalyst was prepared by impregnated cobalt nitrate onto the TiO_2 support having the higher amount of bulk defect and lower amount of surface defect. However, the reduction temperatures did not follow the trends on the sample Co/TiO_2-C showing lower reduction temperature than the expectation, especially on the 2nd reduction peak, which exhibited the lowest reduction temperature among other samples. As suggested, the electron on cobalt of Co/TiO_2-E should be rich at cobalt-TiO_2 interface. Therefore, it can be suggested that the electron of oxygen atom of Co_3O_4 should also be rich at the interface between cobalt atom and oxygen atom resulting in irremovable oxygen atom. However, on contrary, for the cobalt sample that was loaded on the TiO_2 support having high bulk defect and low surface defect, the reduction temperature also became higher. This could be attributed to low SMSI and low surface defect leading to being easy for cobalt migration on the TiO_2 support causing of the formation of cobalt-support compound resulting being more difficult to reduce the Co_3O_4 to Co^o [3].
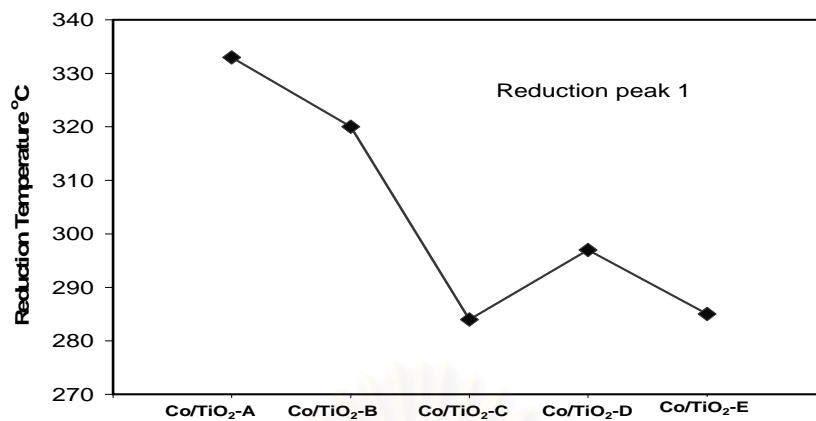
(a) Reduction peak 1
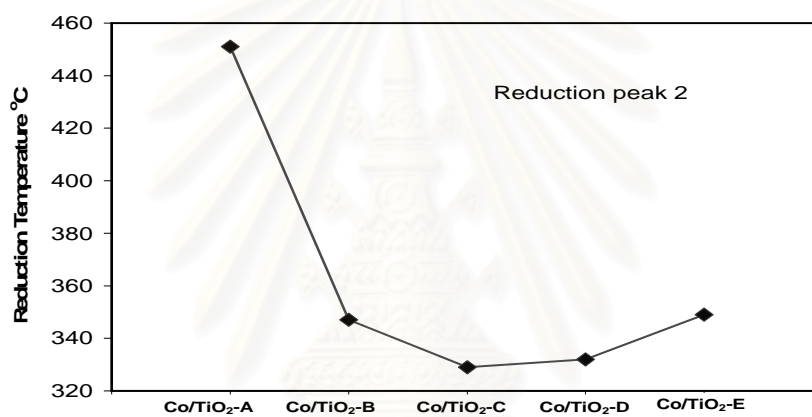
(b) Reduction peak 2
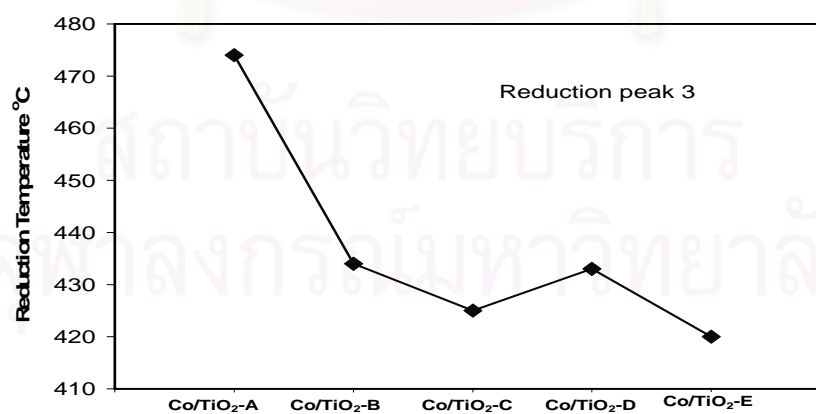
(c) Reduction peak3

Figure 5.9 Reduction Temperature of Co/TiO_2 catalysts

5.4 Catalytic activity for CO-hydrogenation over Co/TiO$_2$ catalyst

To determine the catalytic behaviors of the supported cobalt catalyst loading on different TiO$_2$ supports, CO hydrogenation (H$_2$/CO = 10/1) under methanation was performed as shown in Table 5.2 . Conversion of CO became higher when the TiO$_2$ having optimum amount of bulk and surface defects was used for supporting the cobalt catalyst. Based on the steady-state rate, it was the highest for the Co/TiO$_2$-C sample and consequently decreased on the Co/TiO$_2$-D and Co/TiO$_2$-E. Considering, the total H$_2$ chemisorption results, it demonstrated that the Co/TiO$_2$-C catalyst can adsorb the highest amount of H$_2$ among other catalysts. Moreover, the reduction temperature also became lower than the expectation (it did not follow the trend) especially on the 2nd reduction peak (became the lowest reduction temperature). This can be attributed to the optimum amounts of bulk and surface defects of TiO$_2$ support was used for preparing Co/TiO$_2$ catalyst by impregnating cobalt nitrate. In addition, it can be observed that high amount of bulk and surface defects also resulted in high selectivity of C$_2$-C$_4$ products during methanation. This was likely due to changes of the nature of active center with high amounts of bulk and surface defects.

Table 5.2 Reaction study

Sample	CO Conversion[a] (%)	Rate[b] (x10^2 gCH$_2$/gcat.h)	Product Selectivity	
			CH$_4$ (%)	C$_2$-C$_4$ (%)
Co/TiO$_2$-A	5	1.9	80	20
Co/TiO$_2$-B	10	3.7	96	4
Co/TiO$_2$-C	70	26.2	98	2
Co/TiO$_2$-D	15	5.6	97	3
Co/TiO$_2$-E	8	3.0	71	29

[a] CO hydrogenation was carried out at 220°C, 1 atm and H$_2$/CO/Ar = 20/2/8

[b] Steady-state rate of –CH$_2$- form as same as moles of CO converted, represented the repeating unit for all hydrocarbon chains in the product stream

CHAPTER VI

CONCLUSIONS AND RECOMMENDATIONS

In this chapter, section 6.1 provides the conclusions obtained from the experimental results of the effects of bulk and surface defects of TiO_2 support on the physico-chemical properties of Co/ TiO_2 catalyst via methanation. Additionally, recommendations for further study are given in section 6.2.

6.1 Conclusions

In this work, the effects of bulk and surface defects on TiO_2 support were investigated over Co/TiO_2 catalyst. It showed that the optimum amount of bulk and surface defects rendered Co/TiO_2 catalyst being high total H_2 chemisorption, high reducibility, low reduction temperature, and consequently high conversion for CO hydrogenation reaction. The selectivity to C_2-C_4 products increased with high bulk and surface defects probably due to changes of the nature of active center.

6.2 Recommendations

1. study eletronic properties change of cobalt after impregnate onto TiO_2 support having different amount of bulk defect and surface defects via methanation.

2. Find the new way to monitor Co dispersion instead H_2-chemisorp

REFERENCES

[1]   Iglesia, E. Design, synthesis, and use of cobalt-based Fischer-Tropsch synthesis catalysts. **Applied Catalysis A**: 161 (1997): 59-78.

[2]   Coville, N.J. and Li, J. Effect of boron source on the catalyst reducibility and Fischer–Tropsch synthesis activity of Co/TiO_2 catalysts. **Catalysis Today** 71 (2002): 403-410.

[3]   Jongsomjit, B.; Sakdamnuson, C.; Goodwin, J.G. and Praserthdam, P. Co-support compound formation in titania-supported cobalt catalyst. **Catalysis Letter** 94 (2004): 209-215.

[4]   Sun, S.; Fujimoto, K.; Zhang, Y. and Tsubaki, N. A highly active and stable Fischer–Tropsch synthesis cobalt/silica catalyst with bimodal cobalt particle distribution. **Catalysis Communications** 4 (2003): 361-364.

[5]   Lu, G., Linsebigler, A. and John T. Yates, Jr. Ti3+ Defect Sites on TiOz(110): Production and Chemical Detection of Active Sites. **Journal of Chemical Physics** 98 (1994): 11733-11738.

[6]   Henrich, V. and Kurtz, R.L. Surface electronic structure of TiO_2: Atomic geometry, ligand coordination, and the effect of adsorbed hydrogen. **Physical Review B** 23 (1981): 6280-6287.

[7]   Suriye, K.; Praserthdam, P. and Jongsomjit, B. Impact of Ti^{3+} Present in Titania on Characteristics and Catalytic Properties of the Co/TiO_2 Catalyst. **Industrial & Engineering Chemistry Research** 44 (2005): 6599-6604.

[8]   Suriye, K.; Praserthdam, P. and Jongsomjit, B. Effect of surface sites of TiO_2 support on the formation of cobalt-support compound in Co/TiO_2 catalysts. **Catalysis Communications** 8 (2007): 1772-1780.

[9]   Suriye, K.; Praserthdam, P. and Jongsomjit, B. Surface defect(Ti3+) controlling on TiO2 nanocrystal using various water:alkoxide molar ratios used during sol-gel synthesis as the first step for surface defect creation. **Applied Surface Science** (sumitted)

[10]   Jung, K.Y. and Park, S.B. Anatase-phase titania: preparation by embedding silica and photocatalytic activity for the decomposition of trichloroethylene. **Journal of Photochemistry and Photobiology A** A 127 (1999): 117-122.

[11]   Yu, J.C.; Yu, J.; Zhang, L. and Hoa, W. Enhancing effects of water content
        and ultrasonic irradiation on the photocatalytic activity of nano-sized
        TiO2 powders. **Journal of Photochemistry and Photobiology A** 148
        (2002): 263-271.

[12]   Trung, T. and Ha, C.S. One-component solution system to prepare nanometric
        anatase TiO_2. **Materials Science and Engineering C** 24 (2004): 19-
        22.

[13]   Wang, C.C. and Ying J.Y. Sol-Gel Synthesis and Hydrothermal Processing of
        Anatase and Rutile Titania Nanocrystals. **Chemistry of Materials** 11
        (1999):3113-3120.

[14]   Duvenhage, D.J. and Coville N.J. $Fe:Co/TiO_2$ bimetallic catalysts for the
        Fischer–Tropsch reaction Part 2. The effect of calcination and
        reduction temperature. **Applied Catalysis A** 233 (2002): 63-75.

[15]   Li, J. and Coville N.J. The effect of boron on the catalyst reducibility and
        activity of Co/TiO_2 Fischer–Tropsch catalysts. **Applied Catalysis A**
        181(1999): 201-208.

[16]   Wang, J.A.; Valenzuela, M.A. and Bokhimi, X. Crystalline structure
        refinements of a series of catalytic materials with the Rietveld
        technique. **Colloids and Surfaces A** 179 (2001): 221-227.

[17]   Wang, J.A.; Limas-Ballesteros, R.; Lopez, T.; Moreno, A.; Gomez, R.;
        Novaro, O. and Bokhimi, X. Quantitative Determination of Titanium
        Lattice Defects and Solid-State Reaction Mechanism in Iron-Doped
        TiO_2 Photocatalysts. **The Journal of Physical Chemistry B** 105
        (2001): 9692-9698.

[18]   Wallace, W.T.; Min, B.K. and Goodman, D.W. The stabilization of supported
        gold clusters by surface defects. **Journal of Molecular Catalysis A**
        228 (2005): 3-10.

[19]   Suriye, K.; Praserthdam, P. and Jongsomjit, B. Control of Ti^{3+} surface defect
        on TiO_2 nanocrystal using various calcination atmospheres as the first
        step for surface defect creation and its application in photocatalysis.
        Applied Surface Science 253 (2007) 3849- 3855.

[20]   Sun, S.; Tsubaki, N. and Fujimoto, K. The reaction performances and
       characterization of Fischer–Tropsch synthesis Co/SiO$_2$ catalysts
       prepared from mixed cobalt salts. **Applied Catalysis A** 202 (2000):
       121-131.

[21]   Diebold, U. The surface science of titanium dioxide. **Surface Science
       Reports** 48 (2003): 53-229.

[22]   Kominami, H.; Kohno, M.; Takada, Y.; Inoue, M.; Inui, T. and Kera, Y.
       Hydrolysis of Titanium Alkoxide in Organic Solvent at High
       Temperatures: A New Synthetic Method for Nanosized, Thermally
       Stable Titanium(IV) Oxide. **Industrial & Engineering Chemistry
       Research** (1999): 3925-3931.

[23]   Resasco, D.E. and Haller, G.L. Metal–Support Interaction: Group VIII Metals
       and Reducible Oxides. **Advances in Catalysis** 36 (1989): 173-235.

[24]   Naccache, C.; Coudurier, G.; Praliaud, H.; Meriaudeau, P.; Gallezot, P.;
       Martin, G.A. and Vedrine, G.C. Studies in Surf. Sci. and Catalysis,
       Vol. 11, **Elsevier 1982.**

[25]   Jongsomjit, B.; Sakdamnuson, C. and Praserthdam, P. Dependence of
       crystalline phases in titania on catalytic properties during CO
       hydrogenation of Co/TiO$_2$ catalysts. **Materials Chemistry and
       Physics** 89 (2005) 395- 401.

[26]   Reuel, R.C. and Bartholomew, C.H. The stoichiometries of H$_2$ and CO
       adsorptions on cobalt: Effects of support and preparation. **Journal of
       Catalysis** 85 (1984) 63-77.

[27]   Yang, J.; Li, D.; Wang, X.; Yang, X. and Lu, L. Synthesis and microstructural
       control of nanocrystalline titania powders via a stearic acid method.
       Materials Science and Engineering A 328 (2002) 108-112.

[28]   Serwicka, E. ESR study on the interaction of water vapour with
       polycrystalline TiO$_2$ under illumination. **Colloids and Surfaces** 13
       (1985) 287-293.

[29]   Lee, S.K.; Robertson, P.K.J.; Mills, A.; McStay, D.; Elliott, N. and McPhail,
       D.The alteration of the structural properties and photocatalytic activity
       of TiO$_2$ following exposure to non-linear irradiation sources. **Applied
       Catalysis B** 44 (2003) 173-184.

[30]   Kutty, T.R.N.; Murugaraj, P. and Gajbhiye, N.S. Activation of trap centres in PTC BaTiO$_3$. **Materials Letters** 2 (1984) 396-400.

[31]   Joung, S.K.; Amemiya, T.; Murabayashi, M. and Itoh, K. Relation between photocatalytic activity and preparation conditions for nitrogen-doped visible light-driven TiO$_2$ photocatalysts. **Applied Catalysis A** 312 (2006) 20-26.

[32]   Nakaoka, Y. and Nosaka, Y. ESR investigation into the effects of heat treatment and crystal structure on radicals produced over irradiated TiO$_2$ powder. **Journal of Photochemistry and Photobiology A** 110 (1997) 299-305.

[33]   Thompson, T.L.; Diwald, O. and Yates, Jr., JT. CO$_2$ as a Probe for Monitoring the Surface Defects on TiO$_2$(110)-Temperature-Programmed Desorption. **The Journal of Physical Chemistry B** 107 (2003) 11700-11704.

[34]   Goodman, D.W. Catalytically active Au on Titania: yet another example of a strong metal support interaction (SMSI)? **Catalysis Letter** 99 (2005) 1-4.

[35]   Wei-xing, X.; Schierbaum, K.D. and Goepel, W. Ab initio study of the effect of oxygen defect on the strong-metal—support interaction between Pt and TiO$_2$(Rutile)(110) surface. **Journal of Solid State Chemistry** 119 (1995) 237-245.

APPENDICES

APPENDIX A

CALCULATION FOR CATALYST PREPARATION

Preparation of TiO$_2$ nanocrystal via sol-gel (based precipitation) method are shown as follows

Reagent:　　-Titanium ethoxide,

　　　　　　Molecular weight = 284.22

　　　　　　-Cobalt (II) nitrate hexahydrate (Co(NO$_3$)$_2 \times$6H$_2$O)

　　　　　　Molecular weight = 290.93

Calculation for the preparation of TiO$_2$ via sol-gel (based precipitation) method

The preparation by using water:alkoxide molar ratio	=	X
Let start with titanium ethoxide	=	10 g
	=	10/284.22 mole
The amount of water used	=	10/284.22×18(X)
The volume of water used	=	10/284.22×18(X)
The volume of ethanol used in the first solution with ethanol	=	50 ml

The volume of ethanol used in thesecond solution with Titanium ethoxide = 50 ml

Calculation for the preparation of cobalt loading catalyst (20%Co/ TiO$_2$)

Base on 100 g of atalyst used, the composition of the catalyst will be as follow:

　　Cobalt　　　=　　20 g

　　TiO$_2$　　　=　　100-20

　　　　　　　=　　80 g

For 5 g of TiO$_2$

　　Cobalt required　　=　　5×(20/80)　　=　　1.25 g

　　Cobalt 1.25 g was prepared from (Co(NO$_3$)$_2 \times$6H$_2$O) and molecular weight of Co is 58.59

Co(NO$_3$)$_2$×6H$_2$O   =   [MW of Co(NO$_3$)$_2$×6H$_2$O×cobalt required]/MW of Co

                =   (290.93/58.93) ×1.25   =   6.17 g

APPENDIX B

CALCULATION FOR TOTAL H₂ CHEMISSORPTION

Calcution of the total H_2 chemisorption and metal dispersion of the catalyst, a stoichiometry of H/Co = 1, measured by H_2 chemisorption is as follows:

Let the weight of catalyst used	=	W	g
Integral area of H_2 peak after adsorption	=	A	unit
Integral area of 45 µl of standard H_2 peak	=	B	unit
Amounts of H_2 adsorbed on catalyst	=	B-A	unit
Volume of H_2 adsorbed on catalyst	=	$45 \times [(B-A)/B]$	µl
Volume of 1 mole of H_2 at 100°C	=	28.038	µl
Mole of H_2 adsorbed on catalyst		$= [(B-A)/B] \times [45/28.038]$	µmole

Total H_2 chemisorption $\quad = [(B-A)/B] \times [45/28.038] \times [1/W]$ µmole/g of catalyst

$\quad\quad\quad\quad\quad\quad\quad\quad = N \quad$ µmole/g of catalyst

APPENDIX C

CALCULATION FOR REDUCIBILITY

For supported cobalt catalyst, it can be assumed that the major species of calcined Co-catalysts is Co_3O_4. H_2 consumption of Co_3O_4 is calculated as follows:
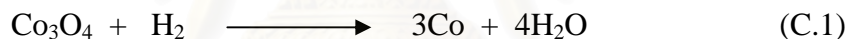
Molecular weight of Co = 58.93

Molecular weight of Co_3O_4 = 240.79

Calculation of the calibration of H_2 consumption using cobalt oxide(Co_3O_4)

Let the weight of Co_3O_4 used $\quad = \quad$ 0.01 g

$\qquad\qquad = \quad 4.153 \times 10^{-5}$ mole

From equation of Co_3O_4 reduction;

$$Co_3O_4 \; + \; H_2 \longrightarrow 3Co \; + \; 4H_2O \qquad\qquad (C.1)$$

$H_2 \quad = \quad 4 \, Co_3O_4$

$\quad = \quad 4 \times 4.153 \times 10^{-5}$

$\quad = \quad 1.661 \times 10^{-4} \quad$ mole

Integral area of Co_3O_4 after reduction $\quad = \quad$ 396572.5 unit

Thus the amount of H_2 that can be consumed at 100 % reducibility is 1.661×10^{-4} mole which releated to the integral area of Co_3O_4 after reduction 396572.5 units.

Calculation of reducibility of supported cobalt catalyst

Integral area of the calcined catalyst $= \quad$ X $\qquad$ unit

The amount of H_2 consumption $\qquad = [1.661 \times 10^{-4} \times (X)/396572.5]$ mole

Let the weight of calcined catalyst used $\quad = \quad$ W $\quad$ g

Concentration of Co $\quad = \quad$ Y $\quad$ %wt

Mole of Co $\qquad = \quad [(W \times Y)/58.93] \qquad$ mole

Mole of Co_3O_4 = $[(W \times Y \times 4)/3 \times 58.93]$ mole

Reducibility (%) of supported Co catalyst =

$$\{[1.661 \times 10^{-4} \times (X)/396572.5] \times 100\}/\{[(W \times Y \times 4)/3 \times 58.93]\}$$

APPENDIX D

CALIBRATION CURVES

This appendix showed the calibration curves for calculation of composition of reactant and products in CO hydrogenation reaction. The reactant is CO and the main product is methane. The other products are linear hydrocarbons of heavier molecular weight that are C_2-C_4 such as ethane, ethylene, propane, propylene and butane.

The thermal conductivity detector, gas chromatography Shimadzu model 8A was used to analyze the concentration of CO by using Molecular sieve 5A column.

The VZ10 column are used with a gas chromatography equipped with a flame ionization detector, Shimadzu model 14B, to analyze the concentration of products including of methane, ethane, ethylene, propane, propylene and butane. Conditions uses in both GC are illustrated in Table D.1.

Mole of reagent in y-axis and area reported by gas chromatography in x-axis are exhibited in the curves. The calibration curves of CO, methane, ethane, ethylene, propane, propylene and butane are illustrated in the following figures.

Table D.1 Conditions use in Shimadzu modal GC-8A and GC-14B.

Parameters	Condition	
	Shimadzu GC-8A	Shimadzu GC-14B
Width	5	5
Slope	50	50
Drift	0	0
Min. area	10	10
T.DBL	0	0
Stop time	50	60
Atten	0	0
Speed	2	2
Method	41	41
Format	1	1
SPL.WT	100	100
IS.WT	1	1
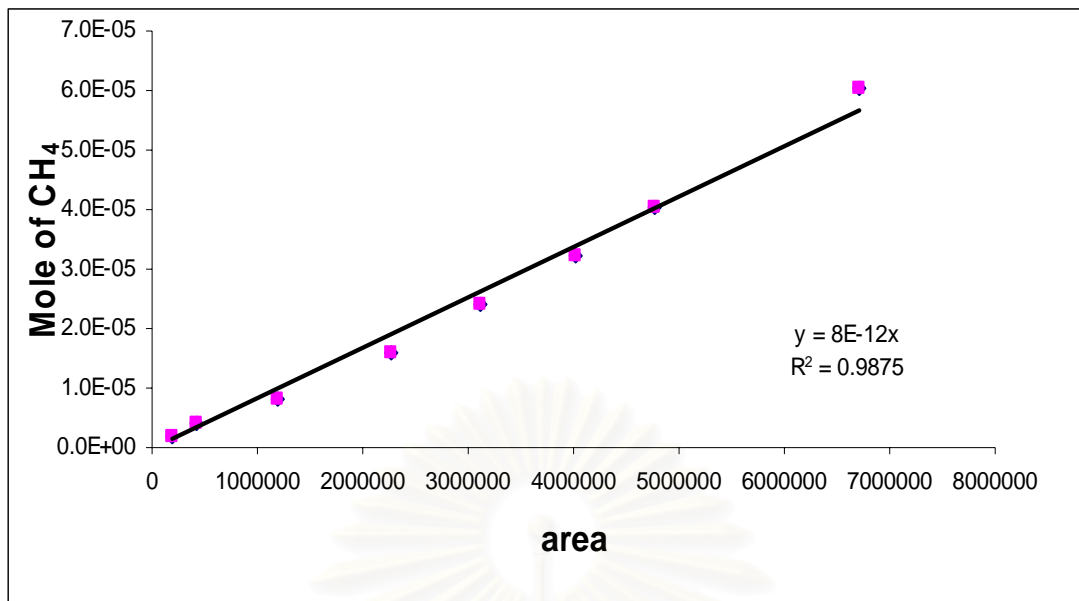
Figure D.1 The calibration curve of methane.
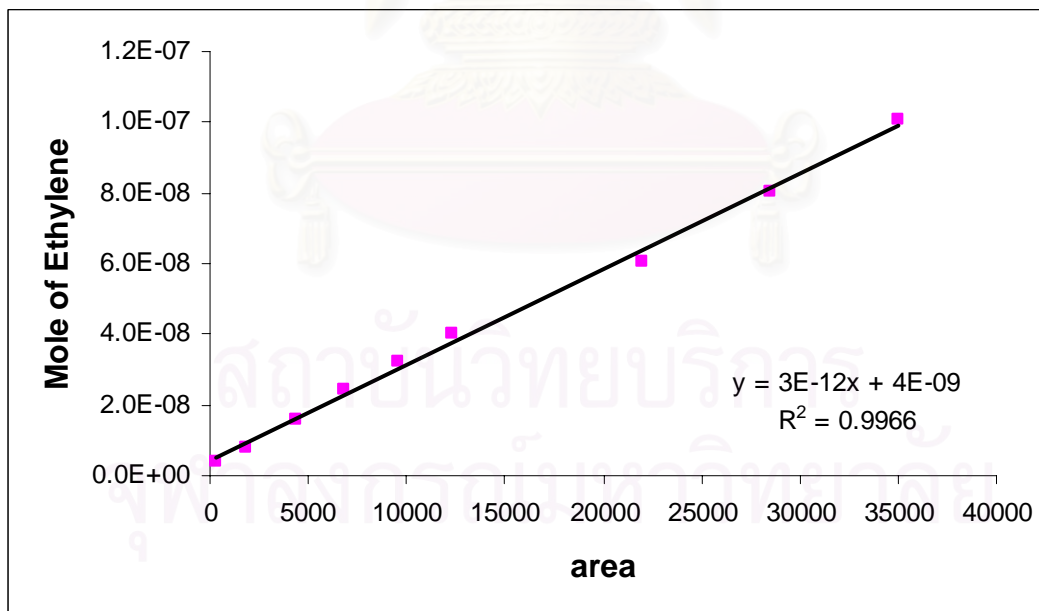
Figure D.2 The calibration curve of ethylene.

C-R8A CHROMATOPAC   CH=1   DATA=1:%CHRM1.C29   ATTEN= 0   SPEED= 2.6

C-R8A CHROMATOPAC CH=1 Report No. 29   DATA=1:%CHRM1.C29   05/12/19 16:53:40

** CALCULATION REPORT **

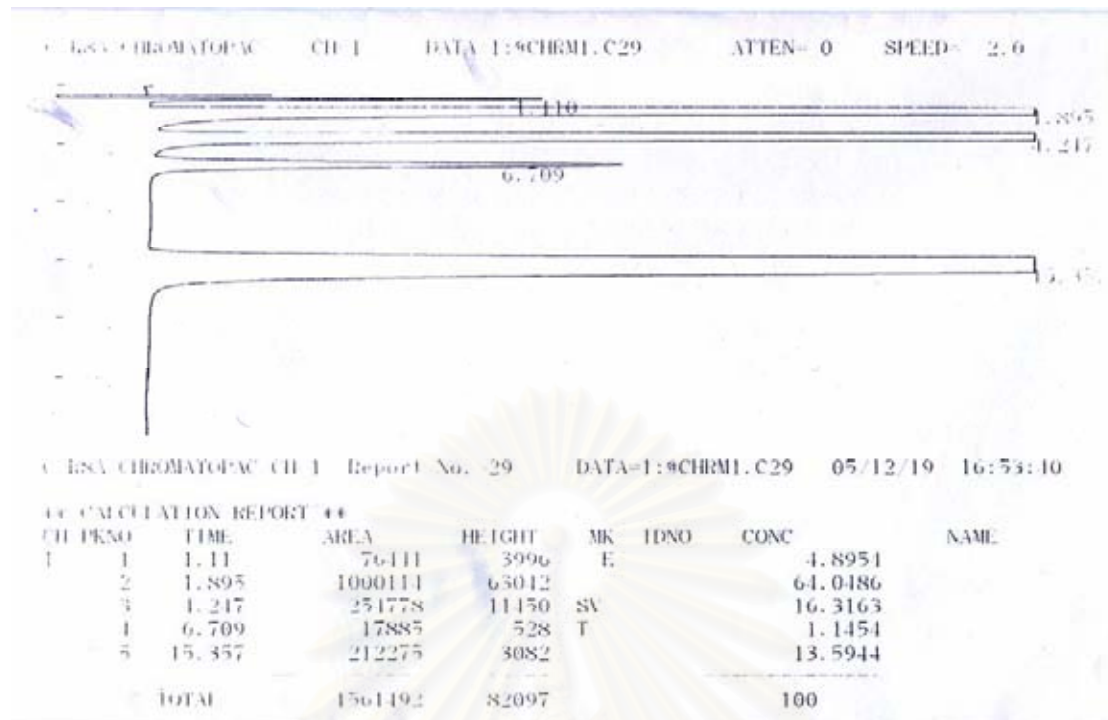| CH	PKNO	TIME	AREA	HEIGHT	MK	IDNO	CONC	NAME
1	1	1.11	76411	3996	E		4.8951	
	2	1.895	1000114	63012			64.0486	
	3	1.247	254778	11450	SV		16.3163	
	4	6.709	17885	528	T		1.1454	
	5	15.357	212275	3082			13.5944	
	TOTAL		1561492	82097			100	

Figure D.3 The chromatograms of catalyst sample from thermal conductivity
detector, gas chromatography Shimadzu model 8A (Molecular sieve 5A
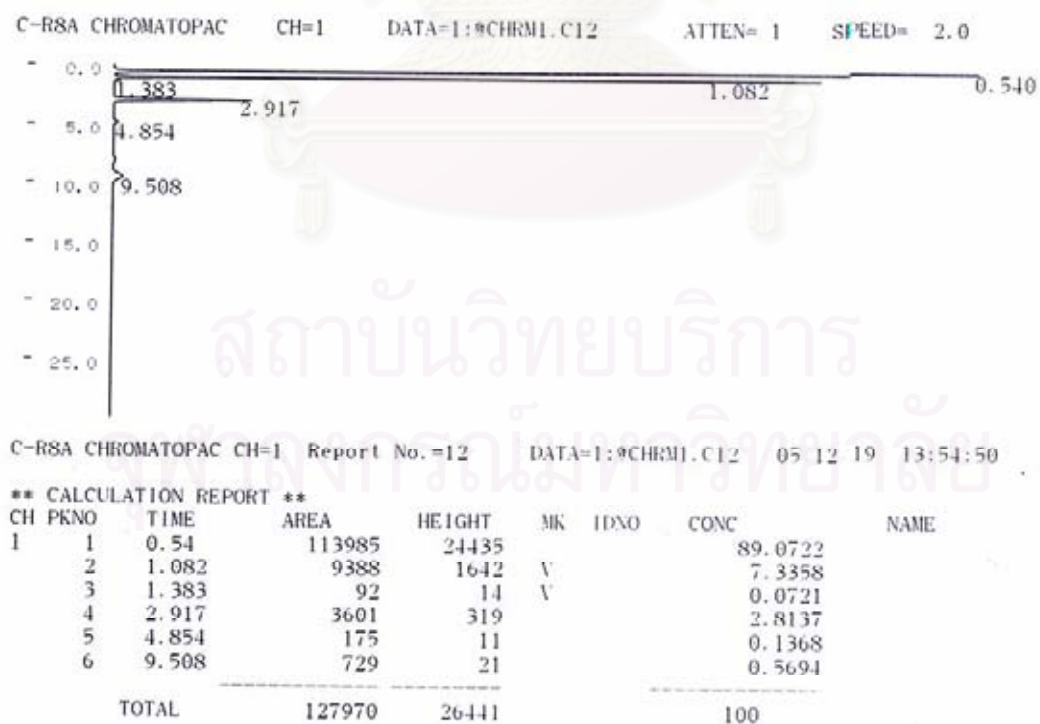column).

C-R8A CHROMATOPAC   CH=1   DATA=1:%CHRM1.C12   ATTEN= 1   SPEED= 2.0

C-R8A CHROMATOPAC CH=1 Report No.=12   DATA=1:%CHRM1.C12   05 12 19 13:54:50

** CALCULATION REPORT **

CH	PKNO	TIME	AREA	HEIGHT	MK	IDNO	CONC	NAME
1	1	0.54	113985	24435			89.0722	
	2	1.082	9388	1642	V		7.3358	
	3	1.383	92	14	V		0.0721	
	4	2.917	3601	319			2.8137	
	5	4.854	175	11			0.1368	
	6	9.508	729	21			0.5694	
	TOTAL		127970	26441			100	

Figure D.4 The chromatograms of catalyst sample from flame ionization detector,
gas chromatography Shimadzu model 14B (VZ10 column).

APPENDIX E

CALCULATION OF CO CONVERSION REACTION RATE AND SELECTIVITY

The catalyst performance for the CO hydrogenation was evaluated in term of activity for CO conversion, reaction rate and selectivity.

CO conversion is defined as moles of CO converted with respect to CO in feed:

$$\text{CO conversion (\%)} = \frac{100 \times [\textit{mole of CO in feed} - \textit{mole of CO in product}]}{\textit{mole of CO in feed}} \quad \text{(i)}$$

For % CO conversion in this thesis as shown in Figure E.

Reaction rate was calculated from CO conversion that is as follows:

Let the weight of catalyst used	=	W	g
Flow rate of CO	=	2	cc/min
Reaction time	=	60	min
Weight of CH_2	=	14	g
Volume of 1 mole of gas at 1 atm	=	22400	cc

$$\text{Reaction rate (g } CH_2/\text{g of catalyst)} = \frac{[\% \textit{ conversion of CO} /100] \times 60 \times 14 \times 2}{W \times 22400} \quad \text{(ii)}$$

Selectivity of product is defined as mole of product (B) formed with respect to mole of CO converted:

$$\text{Selectivity of B (\%)} = 100 \times [\textit{mole of B formed} / \textit{mole of total products}] \quad \text{(iii)}$$

Where B is product, mole of B can be measured employing the calibration curve of products such as methane, ethane, ethylene, propane, propylene and butane

$$\text{mole of } CH_4 = \text{(area of } CH_4 \text{ peak from integrator plpt on GC-14B) x } 8*10^{12} \quad \text{(iv)}$$
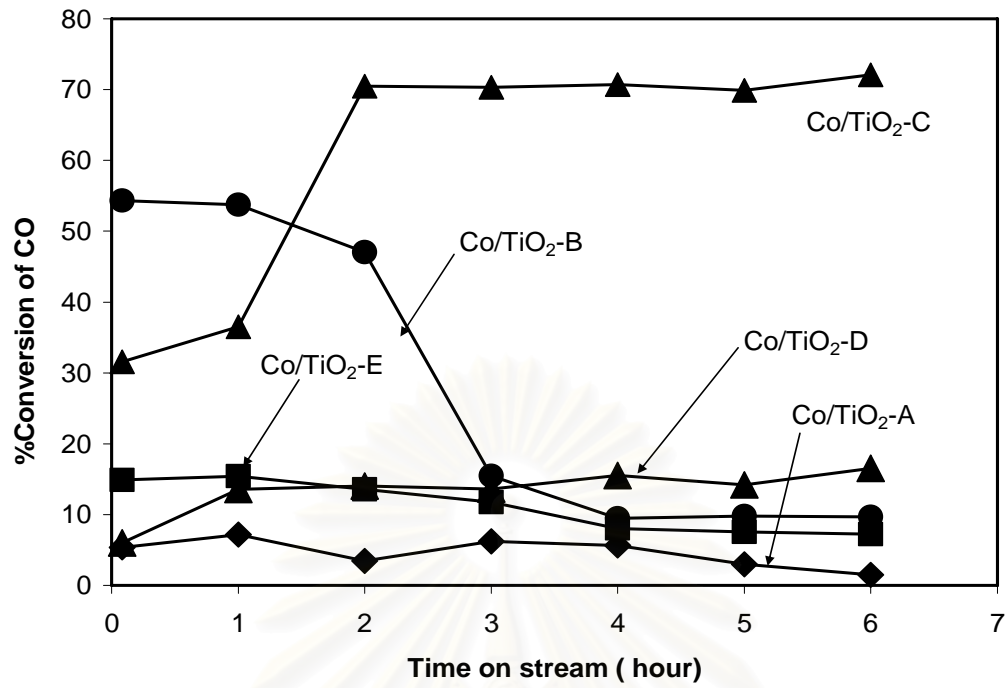
Figure E The reaction study in CO hydrogenation of Co/TiO$_2$ catalyst

APPENDIX F

THERMAL ANALYSIS

Thermal gravimetric analysis (TGA) was adopted to evaluate the weight loss of all as-synthesized Co/TiO_2 samples before calcination (did not show all). The TGA curves of Co/TiO_2-A, Co/TiO_2-C, and Co/TiO_2-D are shown in Figure F.
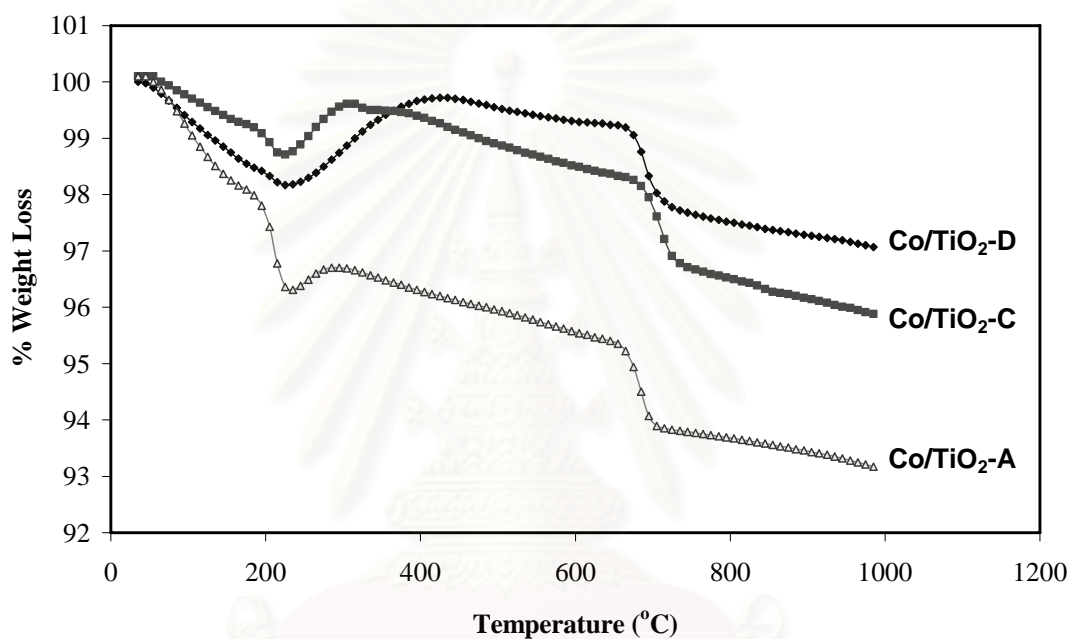

Figure F Thermal gravimetric analysis Of Co/TiO_2 catalyst

APPENDIX G

PROCEEDING

- **Proceeding**

Supawan Supawanitchmongkol, Bunjerd Jongsomjit, and Piyasan Ptaserthdam, "Effects of bulk and surface defects of TiO_2 support on the physico-chemical properties of Co/TiO_2 catalyst via methanation", Proceeding of the 17th Thailand Chemical Engineering and Applied Chemistry Conference, Chiangmai Thailand, Oct., 2007.

- **International Papers**

Supawan Supawanitchmongkol, Piyasan Praserthdam, and Bunjerd Jongsomjit, "Effects of bulk and surface defects of TiO_2 support on the physico-chemical properties of Co/TiO_2 catalyst via methanation", Repaired to Journal of molecular catalysis A.

VITA

Miss Supawan Supawanitchmongkol was born on 31th May 1983, in Bangkok, Thailand. She finished high school from Mahapruttaram girl's school, Bangkok in 2002, and received her Bachelor degree of Chemical Enginerring from Faculty of Engineer, King Mongut's university of Technology Thonburi, Thailand in March 2006. She continued her Master's study at the department of Chemical Engineering, Faculty of Engineering, Chulalongkorn University in 2006.